Influence of Zig-Zag and warping effects on buckling of functionally graded sandwich plates according to sinusoidal shear deformation theories

Publisher copyright

(Article begins on next page)

29 November 2022

Influence of Zig-Zag and warping effects on buckling of functionally graded sandwich plates according to sinusoidal shear deformation theories

A. M. A. Neves, A. J. M. Ferreira, E. Carrera, M. Cinefra, R. M. N. Jorge, C. M. Mota Soares & A. L. Araújo

Accepted author version posted online: 31 May 2016.
Published online: 31 May 2016.

Submit your article to this journal ↗

View related articles ↗

View Crossmark data ↗

Influence of Zig-Zag and warping effects on buckling of functionally graded sandwich plates according to sinusoidal shear deformation theories

A. M. A. Neves [b], A. J. M. Ferreira [a], E. Carrera [c], M. Cinefra [c], R. M. N. Jorge [a], C. M. M. Soares [d], A. L. Araújo [d]

[a]*Departamento de Engenharia Mecânica, Faculdade de Engenharia, Universidade do Porto, Rua Dr. Roberto Frias, 4200-465 Porto, Portugal*

[b]*(Corresponding author: ananeves@fe.up.pt)*
Departamento de Engenharia Mecânica, Faculdade de Engenharia, Universidade do Porto, Rua Dr. Roberto Frias, 4200-465 Porto, Portugal

[c]*Departament of Aeronautics and Aerospace Engineering, Politecnico di Torino, Corso Duca degli Abruzzi, 24, 10129 Torino, Italy*

[d]*Instituto Superior Técnico, Av. Rovisco Pais, Lisboa, Portugal*

Abstract

In this paper various sinusoidal shear deformation theories are used for the buckling analysis of functionally graded sandwich plates. The theories may account for through-the-thickness deformations and/or Zig-Zag effect.

The governing equations and boundary conditions are derived using the Principle of Virtual Work under a generalization of Carrera's Unified Formulation and further interpolated by collocation with radial basis functions.

A numerical investigation has been conducted on the buckling analysis of sandwich plates with functionally graded skins. The influence of the thickness stretching and the Zig-Zag effects on these problems is investigated. Numerical results demonstrate the accuracy of the present approach.

Keywords: Buckling; plates; Functionally graded materials; meshless methods; Zig-Zag effects; warping effects; sinusoidal shear deformation theories.

1 Introduction

The buckling phenomenon consists of a sudden change of equilibrium geometry at a certain critical load. It is one of the characteristic failure modes of slender structures such as laminated composite plates.

Functionally graded (FG) materials were first proposed by Bever and Duwez [1] in 1972. The modelling of FG materials is important to understand the behavior of FG structures.

When compared to isotropic and laminated plates, the literature on FG plates is relatively scarce [2,3] [4–7] [8]. The thermo-mechanical response of FG plates was considered by Reddy and Chin [9], Reddy [10], Vel and Batra [11,12], Cheng and Batra [13], Javaheri and Eslami [14]. Studies on the mechanical behaviour of FG plates include the static analysis of FG plates performed by Kashtalyan [15], Kashtalyan and Menshykova [16], Qian et al. [17], Zenkour [18,19], Ramirez et al. [20], Ferreira et al. [21,22], Chi and Chung [23,24], and Cheng and Batra [25]. Vibrations problems of FG plates can be found in Batra and Jin [26], Ferreira et al. [27], Vel and Batra [28], Zenkour [29], Roque et al. [30], and Cheng and Batra [31]. Mechanical buckling of FG plates can be found in Najafizadeh and Eslami [32], Zenkour [29], Cheng and Batra [31], Birman [33], Javaheri and Eslami [34].

Most of the shear deformation theories neglect the thickness stretching ϵ_{zz}, being the transverse displacement considered to be independent of thickness coordinates. The effect of thickness stretching in FG plates has been recently investigated by Carrera et al. [35]. The zig-zag effect is produced by the large difference of mechanical properties of sandwich skins and core. For sandwich plates, the classical plate theories of Kirchhoff [36] or Reissner-Mindlin [37,38] present some difficulties. Two possibilities can be used to capture the ZZ effect (see the overviews by Burton and Noor [39], Noor et al. [40], Altenbach [41], Librescu and Hause [42], Vinson [43], and Demasi [44]): the so-called layer-wise models, and a zig-zag function (ZZF) in the framework of mixed multilayered plate theories. An historical review on ZZ theories has been provided by Carrera [45].

In order to avoid the computationally expensive layerwise theories, Murakami [46] proposed a ZZF that is able to reproduce the slope discontinuity. A review of early developments on the application of ZZF has been provided in the review article by Carrera [47]. The advantages of analysing multilayered anisotropic plate and shells using the ZZF as well as the Finite Element implementation have been discussed by Carrera [48], and by others [48–50].

This paper focus on the buckling analysis of functionally graded sandwich plates. It adresses the influence of the warping effects in the thickness direction as well as the Zig-Zag (ZZ) effects on these problems. Four sinusoidal theories are used. The governing equations and boundary conditions are derived under a generalized version of Carrera's Unified Formulation (CUF) [51,47] based on the principle of virtual displacements and further interpolated by collocation with radial basis functions (RBF). This meshless technique can be seen as an efficient alternative to the finite elements method [52–55] [56–59] [60,61].

2   Problem formulation

A rectangular sandwich plate of plan-form dimensions a and b and uniform thickness h is considered. The co-ordinate system is taken such that the x-y plane ($z = 0$) coincides with the midplane of the plate.

The sandwich core is fully ceramic (isotropic) and skins are composed of a functionally graded material across the thickness direction. The bottom skin varies from a metal-rich surface ($z = -h/2$) to a ceramic-rich surface while the top skin face varies from a ceramic-rich surface to a metal-rich surface ($z = h/2$) as illustrated in figure 1. There are no interfaces between core and skins. The volume fraction of the ceramic phase is obtained from a simple rule of mixtures as:

$$\begin{cases} V_c = \left(\frac{z-h_0}{h_1-h_0}\right)^p & \text{in the bottom skin} \\ V_c = 1 & \text{in the core} \\ V_c = \left(\frac{z-h_3}{h_2-h_3}\right)^p & \text{in the top skin} \end{cases} \tag{1}$$

where $z \in [-h/2, h/2]$, h_0, h_1, h_2, and h_3 are the z-coordinates of the interfaces of the layers as visualized in figure 1, and $p \geq 0$ is a scalar parameter that allows the user to define gradation of material properties across the thickness direction of the skins. The $p = 0$ case corresponds to the (isotropic) fully ceramic plate. The volume fraction for the metal phase is given as $V_m = 1 - V_c$.

The sandwiches may be symmetric or non-symmetric about the mid-plane as we may vary the thickness of each face. Figure 2 shows a non-symmetric sandwich with volume fraction defined by the power-law (1) for various exponents p, in which top skin thickness is the same as the core thickness and the bottom skin thickness is twice the core thickness. Such thickness relation is denoted as 2-1-1. A bottom-core-top notation is being used. 1-1-1 means that skins and core have the same thickness. The sandwich plate is subjected to compressive in-plane forces acting on the

mid-plane of the plate. $\bar{N}_{xx}$ and $\bar{N}_{yy}$ denote the in-plane loads perpendicular to the edges $x = 0$ and $y = 0$ respectively, and $\bar{N}_{xy}$ denote the distributed shear force parallel to the edges $x = 0$ and $y = 0$ respectively (see fig. 3).

3   Overview of existing zig-zag theories

The Murakami's zig-zag function $Z(z)$ dependes on the adimensioned layer coordinate, ζ_k, according to the following formula:

$$Z(z) = (-1)^k \zeta_z \tag{2}$$

ζ_k is defined as $\zeta_k = \frac{2z_k}{h_k}$ where z_k is the layer coordinate in the thickness direction and h_k is the thickness of the kth layer.

$Z(z)$ has the following properties:

(1) It is a piece-wise linear function of layer coordinates z_k,
(2) $Z(z)$ has unit amplitude for the whole layers,
(3) the slope $Z'(z) = \frac{dZ}{dz}$ assumes opposite sign between two-adjacent layers. Its amplitude is layer thickness independent.

In 1986, a refinement of FSDT by inclusion of ZZ effects and transverse normal strains was introduced in Murakami's original ZZF [46], defined by the following displacement field:

$$\begin{cases} u = u_0 + z u_1 + (-1)^k \frac{2}{h_k} \left(z - \frac{1}{2} (z_k + z_{k+1}) \right) u_Z \\ v = v_0 + z v_1 + (-1)^k \frac{2}{h_k} \left(z - \frac{1}{2} (z_k + z_{k+1}) \right) v_Z \\ w = w_0 + z w_1 + (-1)^k \frac{2}{h_k} \left(z - \frac{1}{2} (z_k + z_{k+1}) \right) w_Z \end{cases} \tag{3}$$

where u and v are the in-plane displacements and w is the transverse displacement. The involved unknowns are u_0, u_1, u_Z, v_0, v_1, v_Z, w_0, w_1, and w_Z: u_0, v_0 and w_0 are translations of a point at the midplane; u_1, v_1 and w_1 are rotations as in the typical FSDT; and the additional degrees of freedom u_Z, v_Z and w_Z have a meaning of displacement. z_k, z_{k+1} are the bottom and top z-coordinates at each layer.

More recently, another possible FSDT theory has been investigated by Carrera [48] and Demasi [49], ignoring the through-the-thickness deformations:

$$
\begin{cases}
u = u_0 + z u_1 + (-1)^k \frac{2}{h_k}\left(z - \frac{1}{2}\left(z_k + z_{k+1}\right)\right) u_Z \\
v = v_0 + z v_1 + (-1)^k \frac{2}{h_k}\left(z - \frac{1}{2}\left(z_k + z_{k+1}\right)\right) v_Z \\
w = w_0
\end{cases}
\tag{4}
$$

with u_0, u_1, u_Z, v_0, v_1, v_Z, w_0, z_k, and z_{k+1} as before.

Ferreira et al. [62] and Rodrigues et al. [63] used a ZZF theory involving the following expansion of displacements

$$
\begin{cases}
u = u_0 + z u_1 + (-1)^k \frac{2}{h_k}\left(z - \frac{1}{2}\left(z_k + z_{k+1}\right)\right) u_Z \\
v = v_0 + z v_1 + (-1)^k \frac{2}{h_k}\left(z - \frac{1}{2}\left(z_k + z_{k+1}\right)\right) v_Z \\
w = w_0 + z w_1 + z^2 w_2
\end{cases}
\tag{5}
$$

This represents a variation of the Murakami's original theory, allowing for a quadratic evolution of the transverse displacement across the thickness direction. Furthermore, Ferreira et al. [64] used two higher order ZZF theories allowing for a quadratic evolution of the transverse displacement across the thickness direction as well and involving the following displacement fields:

$$
\begin{cases}
u = u_0 + z u_1 + z^3 u_3 + (-1)^k \frac{2}{h_k}\left(z - \frac{1}{2}\left(z_k + z_{k+1}\right)\right) u_Z \\
v = v_0 + z v_1 + z^3 v_3 + (-1)^k \frac{2}{h_k}\left(z - \frac{1}{2}\left(z_k + z_{k+1}\right)\right) v_Z \\
w = w_0 + z w_1 + z^2 w_2
\end{cases}
\tag{6}
$$

The use of a sinusoidal shear deformation theory for composite laminated plates and shells was first presented by Touratier [65,66] [67] in the early 1990's. Later Vidal and Polit [68] used a sinusoidal shear deformation theory for composite laminated beams. The use of sinusoidal plate theories for functionally graded plates was first presented by Zenkour [19], where a $\epsilon_{zz} = 0$ approach was used. Recently Neves et al. [60,61] successfully used a sinusoidal plate theory for the bending and stress analysis of functionally graded plates.

$$
\begin{cases}
u = u_0 + z u_1 + sin\left(\frac{\pi z}{h}\right) u_3 + (-1)^k \frac{2}{h_k}\left(z - \frac{1}{2}\left(z_k + z_{k+1}\right)\right) u_Z \\
v = v_0 + z v_1 + sin\left(\frac{\pi z}{h}\right) v_3 + (-1)^k \frac{2}{h_k}\left(z - \frac{1}{2}\left(z_k + z_{k+1}\right)\right) v_Z \\
w = w_0 + z w_1 + z^2 w_2
\end{cases}
\tag{7}
$$

All previous cited work using ZZ functions deals with laminated plates or shells. Refering to functionally graded sandwiches, the authors have sucessfuly used two hyperbolic-sine shear deformation theories for the static study of functionally graded sandwich plates [69]. They both account for the Zig-Zag effect, but only one allows for warping in the thickness direction:

$$
\begin{cases}
u = u_0 + z u_1 + \sinh\left(\frac{\pi z}{h}\right) u_3 + (-1)^k \frac{2}{h_k}\left(z - \frac{1}{2}(z_k + z_{k+1})\right) u_Z \\
v = v_0 + z v_1 + \sinh\left(\frac{\pi z}{h}\right) v_3 + (-1)^k \frac{2}{h_k}\left(z - \frac{1}{2}(z_k + z_{k+1})\right) v_Z \\
w = w_0
\end{cases}
\tag{8}
$$

$$
\begin{cases}
u = u_0 + z u_1 + \sinh\left(\frac{\pi z}{h}\right) u_3 + (-1)^k \frac{2}{h_k}\left(z - \frac{1}{2}(z_k + z_{k+1})\right) u_Z \\
v = v_0 + z v_1 + \sinh\left(\frac{\pi z}{h}\right) v_3 + (-1)^k \frac{2}{h_k}\left(z - \frac{1}{2}(z_k + z_{k+1})\right) v_Z \\
w = w_0 + z w_1 + z^2 w_2
\end{cases}
\tag{9}
$$

4 The present sinus shear deformation theories

In this paper we compare four sinusoidal shear deformation theories. In-plane displacements (u, v) are considered to be of sinusoidal type across the thickness coordinate and may include or not the terms to account for the zig-zag effect. The transverse displacement (w) may be defined as constant if warping is not allowed, or as parabolic in the thickness direction if warping is allowed.

For the easy reading of the paper, nomenclature is now introduced. All theories are named *sinus*, as they all consider a sinusoidal expansion across the thickness coordinate for the in-plane displacements. In addition the name will include the *ZZ* letters if the zig-zag effect is considered, and will include the 0 number if $\epsilon_{zz} = 0$, i. e., thickness-stretching is not allowed (see table 1).

The displacement fields of each theory are as follows:

Displacement field of sinus theory:

$$
\begin{cases}
u = u_0 + z u_1 + \sin\left(\frac{\pi z}{h}\right) u_s \\
v = v_0 + z v_1 + \sin\left(\frac{\pi z}{h}\right) v_s \\
w = w_0 + z w_1 + z^2 w_2
\end{cases}
\tag{10}
$$

Displacement field of sinus0 theory:

$$\begin{cases} u = u_0 + zu_1 + \sin\left(\frac{\pi z}{h}\right) u_s \\ v = v_0 + zv_1 + \sin\left(\frac{\pi z}{h}\right) v_s \\ w = w_0 \end{cases} \tag{11}$$

Displacement field of sinusZZ theory:

$$\begin{cases} u = u_0 + zu_1 + \sin\left(\frac{\pi z}{h}\right) u_s + (-1)^k \frac{2}{h_k}\left(z - \frac{1}{2}\left(z_k + z_{k+1}\right)\right) u_Z \\ v = v_0 + zv_1 + \sin\left(\frac{\pi z}{h}\right) v_s + (-1)^k \frac{2}{h_k}\left(z - \frac{1}{2}\left(z_k + z_{k+1}\right)\right) v_Z \\ w = w_0 + zw_1 + z^2 w_2 \end{cases} \tag{12}$$

Displacement field of sinusZZ0 theory:

$$\begin{cases} u = u_0 + zu_1 + \sin\left(\frac{\pi z}{h}\right) u_s + (-1)^k \frac{2}{h_k}\left(z - \frac{1}{2}\left(z_k + z_{k+1}\right)\right) u_Z \\ v = v_0 + zv_1 + \sin\left(\frac{\pi z}{h}\right) v_s + (-1)^k \frac{2}{h_k}\left(z - \frac{1}{2}\left(z_k + z_{k+1}\right)\right) v_Z \\ w = w_0 \end{cases} \tag{13}$$

The expansion of the degrees of freedom u_0, u_1, u_s, v_0, v_1, v_s, w_0, w_1, and w_2 are functions of the thickness coordinate only. These are layer-independent, unlike those of u_Z and v_Z, as illustrated in figures 4 and 5.

5 The Unified Formulation for the buckling analysis of FG sandwich plates

In this section it is shown how to obtain the fundamental nuclei under CUF, which allows the derivation of the governing equations and boundary conditions for FG plates.

5.1 Functionally graded materials

A conventional FG plate considers a continuous variation of material properties over the thickness direction by mixing two different materials [2]. The material properties of the FG plate are assumed to change continuously throughout the thickness of the plate, according to the volume fraction of the constituent materials. Although one can use CUF for one-layer, isotropic plate, we consider a multi-layered plate. In fact, the sandwiches in study present 3 physical layers, $kp = 1, 2, 3,$

and depending on the considered theory may have different displacement fields. Nevertheless, we are dealing with functionally graded materials and becomes mandatory to model the continuos variation of properties across the thickness direction. A considerable number of layers is needed to ensure correct computation of material properties at each thickness position, and for that reason we consider a total of $N_l = 91$ virtual (mathematical) layers of constant thickness for the entire plate of thickness h. In the following, kp refers to physical layers and $k = 1, ..., 91$ refers to virtual layers.

The CUF procedure applied to FG materials starts by evaluating the volume fraction of the two constituents for each layer. To describe the volume fractions an exponential function can be used as in [70], or the sigmoid function as proposed in [71]. In the present work a power-law function is used as most researchers do [72] [32,18,19]. In the typical FG plate the power-law function defines the volume fraction of the ceramic phase as:

$$V_c = \left(0.5 + \frac{z}{h}\right)^p \tag{14}$$

where $z \in [-h/2, h/2]$, h is the thickness of the plate, and p is a scalar parameter that allows the user to define gradation of material properties across the thickness direction. In the present sandwich plate, the volume fraction of the ceramic phase of the FG skins are obtained by adapting the typical power-law. Furthermore, we need to compute the volume fraction for each layer. Considering (1), one has:

$$\begin{cases} V_c^k = \left(\frac{\tilde{z}-h_0}{h_1-h_0}\right)^p, & z \in [h_0, h_1] \\ V_c^k = 1, & z \in [h_1, h_2] \\ V_c^k = \left(\frac{\tilde{z}-h_3}{h_2-h_3}\right)^p, & z \in [h_2, h_3] \end{cases} \tag{15}$$

where $\tilde{z}$ is the thickness coordinate of a point of each (virtual) skin layer, and h_0, h_1, h_2, h_3, and $p \geq 0$ are as in (1).

Having the volume fraction of each constituent, a homogenization procedure is employed to find the values of the modulus of elasticity, E^k, and Poisson's ratio, ν^k, of each layer. A possible homogenization technique is the Mori-Tanaka one [73,74], and other possibility is the law-of-mixtures. In the present work we use the last one so that we can compare our results with referenced authors. The law-of-mixtures states that:

$$E^k(z) = E_m V_m + E_c V_c; \qquad \nu^k(z) = \nu_m V_m + \nu_c V_c \tag{16}$$

where $E^k(z)$ and $\nu^k(z)$ are the $k - th$ layer homogeneized modulus of elasticity and Poisson's ratio,

E_m and E_c are the modulus of elasticity for metal and ceramic phases, respectively, V_m and V_c are the corresponding volume fractions, and v_m and v_c are the Poisson's ratios for metal and ceramic phases.

5.2 Displacements

According to the Unified Formulation by Carrera, the three displacement components u_x, $u_y(=v)$ and $u_z(=w)$ and their relative variations are modeled as:

$$(u_x, u_y, u_z) = F_\tau\ (u_{x\tau}, u_{y\tau}, u_{z\tau}) \qquad (\delta u_x, \delta u_y, \delta u_z) = F_s\ (\delta u_{xs}, \delta u_{ys}, \delta u_{zs}) \tag{17}$$

The vectors are chosen by resorting to the displacement field. In the present formulation the thickness functions of each theory are as follows

sinus theory:

$$\begin{cases} F_{sux} = F_{suy} = F_{\tau ux} = F_{\tau uy} = \begin{bmatrix} 1 & z & \sin\left(\frac{\pi z}{h}\right) \end{bmatrix} \\ F_{suz} = F_{\tau uz} = \begin{bmatrix} 1 & z & z^2 \end{bmatrix} \end{cases} \tag{18}$$

sinus0 theory:

$$\begin{cases} F_{sux} = F_{suy} = F_{\tau ux} = F_{\tau uy} = \begin{bmatrix} 1 & z & \sin\left(\frac{\pi z}{h}\right) \end{bmatrix} \\ F_{suz} = F_{\tau uz} = [1] \end{cases} \tag{19}$$

sinusZZ theory:

$$\begin{cases} F_{sux} = F_{suy} = F_{\tau ux} = F_{\tau uy} = \begin{bmatrix} 1 & z & \sin\left(\frac{\pi z}{h}\right) & (-1)^{kp}\frac{2}{h_{kp}}\left(z - \frac{1}{2}\left(z_{kp} + z_{kp+1}\right)\right) \end{bmatrix} \\ F_{suz} = F_{\tau uz} = \begin{bmatrix} 1 & z & z^2 \end{bmatrix} \end{cases} \tag{20}$$

sinusZZ0 theory:

$$\begin{cases} F_{sux} = F_{suy} = F_{\tau ux} = F_{\tau uy} = \begin{bmatrix} 1 & z & \sin\left(\frac{\pi z}{h}\right) & (-1)^{kp}\frac{2}{h_{kp}}\left(z - \frac{1}{2}\left(z_{kp} + z_{kp+1}\right)\right) \end{bmatrix} \\ F_{suz} = F_{\tau uz} = [1] \end{cases} \tag{21}$$

The present formulation can be seen as a generalization of the original Carrera's Unified Formulation in the sense that different expansions for the in-plane and the out-of-plane displacement are considered.

5.3 Strains

Stresses and strains are separated into in-plane and normal components, denoted respectively by the subscripts p and n.

The geometrical relations (G) between the mechanical strains in the kth layer and the displacement field $\mathbf{u}^k = \{u_x^k, u_y^k, u_z^k\}$ depend on the option of considering or not the warping in thickness direction.

For the *sinus* and *sinusZZ* theories, G can be stated as follows:

$$\epsilon_{pG}^k = [\epsilon_{xx}, \epsilon_{yy}, \gamma_{xy}]^{kT} = \mathbf{D}_p^{k(nl)}\mathbf{u}^k \ , \tag{22}$$

$$\epsilon_{nG}^k = [\gamma_{xz}, \gamma_{yz}, \epsilon_{zz}]^{kT} = (\mathbf{D}_{np}^k + \mathbf{D}_{nz}^k) \ \mathbf{u}^k \ ,$$

wherein the differential operator arrays are defined as follows:

$$\mathbf{D}_p^{k(nl)} = \begin{bmatrix} \partial_x & 0 & \partial_x^2/2 \\ 0 & \partial_y & \partial_y^2/2 \\ \partial_y & \partial_x & \partial_x\partial_y \end{bmatrix} , \quad \mathbf{D}_{np}^k = \begin{bmatrix} 0 & 0 & \partial_x \\ 0 & 0 & \partial_y \\ 0 & 0 & 0 \end{bmatrix} , \quad \mathbf{D}_{nz}^k = \begin{bmatrix} \partial_z & 0 & 0 \\ 0 & \partial_z & 0 \\ 0 & 0 & \partial_z \end{bmatrix} , \tag{23}$$

Although one needs to account for the nonliner contributions for the buckling analysis, we can use the linear version of CUF as the non-linear terms will only influence the equation refering to δw_0. In fact, the compressive in-plane forces and distributed shear forces only actuate on the mid-plane ($z = 0$) and the nonlinear terms are reduced to $\frac{1}{2}\left(\frac{\partial w_0}{\partial x}\right)^2$, $\frac{1}{2}\left(\frac{\partial w_0}{\partial y}\right)^2$, and $\frac{\partial w_0}{\partial x}\frac{\partial w_0}{\partial y}$.

For the *sinus* and *sinusZZ* theories ($\epsilon_{zz} \neq 0$, i.e., warping is allowed), we use

$$\mathbf{D}_p^k = \begin{bmatrix} \partial_x & 0 & 0 \\ 0 & \partial_y & 0 \\ \partial_y & \partial_x & 0 \end{bmatrix} \tag{24}$$

instead of $\mathbf{D}_p^{k(nl)}$ and just add the terms in referred equation.

For the *sinus*0 and *sinusZZ*0 theories ($\epsilon_{zz} = 0$, i.e., warping is not allowed), ϵ_{pG}^k and the differential operator array $\mathbf{D}_p^k$ remain as before, but the other strains are reduced to

$$\epsilon_{nG}^k = [\gamma_{xz}, \gamma_{yz}]^{kT} = (\mathbf{D}_{np}^k + \mathbf{D}_{nz}^k) \ \mathbf{u}^k \ , \tag{25}$$

wherein the differential operator arrays are defined as:

$$\mathbf{D}_{np}^k = \begin{bmatrix} 0 & 0 & \partial_x \\ 0 & 0 & \partial_y \end{bmatrix}, \quad \mathbf{D}_{nz}^k = \begin{bmatrix} \partial_z & 0 & 0 \\ 0 & \partial_z & 0 \end{bmatrix}, \tag{26}$$

5.4 Elastic stress-strain relations

To define the constitutive equations (C), stresses are separated into in-plane and normal components as well. The elastic stress-strain relations depend on which assumption of ϵ_{zz} we consider.

For the *sinus* and *sinusZZ* theories, the 3D constitutive equations are used:

$$\sigma_{pC}^k = [\sigma_{xx}, \sigma_{yy}, \sigma_{xy}]^{kT} = \mathbf{C}_{pp}^k \, \epsilon_{pG}^k + \mathbf{C}_{pn}^k \, \epsilon_{nG}^k \qquad \sigma_{nC}^k = [\sigma_{xz}, \sigma_{yz}, \sigma_{zz}]^{kT} = \mathbf{C}_{np}^k \, \epsilon_{pG}^k + \mathbf{C}_{nn}^k \, \epsilon_{nG}^k \tag{27}$$

with

$$\mathbf{C}_{pp}^k = \begin{bmatrix} C_{11}^k & C_{12}^k & 0 \\ C_{12}^k & C_{11}^k & 0 \\ 0 & 0 & C_{44}^k \end{bmatrix} \qquad \mathbf{C}_{pn}^k = \begin{bmatrix} 0 & 0 & C_{12}^k \\ 0 & 0 & C_{12}^k \\ 0 & 0 & 0 \end{bmatrix} \quad \mathbf{C}_{np}^k = \begin{bmatrix} 0 & 0 & 0 \\ 0 & 0 & 0 \\ C_{12}^k & C_{12}^k & 0 \end{bmatrix} \qquad \mathbf{C}_{nn}^k = \begin{bmatrix} C_{44}^k & 0 & 0 \\ 0 & C_{44}^k & 0 \\ 0 & 0 & C_{11}^k \end{bmatrix} \tag{28}$$

and the C_{ij}^k are the three-dimensional elastic constants

$$C_{11}^k = \frac{E^k(1-(\nu^k)^2)}{1-3(\nu^k)^2-2(\nu^k)^3}; \quad C_{12}^k = \frac{E^k(\nu^k+(\nu^k)^2)}{1-3(\nu^k)^2-2(\nu^k)^3}; \quad C_{44}^k = \frac{E^k}{2(1+\nu^k)} \tag{29}$$

where the modulus of elasticity and Poisson's ratio were defined in (16).

For the *sinus*0 and *sinusZZ*0 theories, as we have $\epsilon_{zz} = 0$, the plane-stress case is used:

$$\sigma_{pC}^k = [\sigma_{xx}, \sigma_{yy}, \sigma_{xy}]^{kT} = \mathbf{C}_{pp}^k \, \epsilon_{pG}^k \qquad\qquad \sigma_{nC}^k = [\sigma_{xz}, \sigma_{yz}]^{kT} = \mathbf{C}_{nn}^k \, \epsilon_{nG}^k \tag{30}$$

with $\mathbf{C}_{pp}^k$ and ϵ_{pG}^k as before, $\epsilon_{nG}^k = [\gamma_{xz}, \gamma_{yz}]^{kT}$ and

$$\mathbf{C}_{nn}^k = \begin{bmatrix} C_{44}^k & 0 \\ 0 & C_{44}^k \end{bmatrix} \tag{31}$$

and C_{ij}^k are the plane-stress reduced elastic constants:

$$C_{11}^k = \frac{E^k}{1 - (\nu^k)^2}; \quad C_{12}^k = \nu^k \frac{E^k}{1 - (\nu^k)^2}; \quad C_{44}^k = \frac{E^k}{2(1 + \nu^k)} \tag{32}$$

5.5 Principle of virtual displacements

In the framework of the Unified Formulation, the Principle of Virtual Displacements (PVD) for the pure-mechanical case is written as:

$$\sum_{k=1}^{N_l} \int_{\Omega_k} \int_{A_k} \left\{ \delta\epsilon_{pG}^k{}^T \sigma_{pC}^k + \delta\epsilon_{nG}^k{}^T \sigma_{nC}^k \right\} d\Omega_k dz = \sum_{k=1}^{N_l} \delta L_e^k \tag{33}$$

where Ω_k and A_k are the integration domains in plane (x,y) and z direction, respectively. As stated before, G means geometrical relations and C constitutive equations, and k indicates the virtual layer. T is the transpose operator and δL_e^k is the external work for the kth layer.

Substituting the geometrical relations (G), the constitutive equations (C), and the modeled displacement field $(F_\tau$ and $F_s)$, all for the kth layer, (33) becomes:

$$\int_{\Omega_k} \int_{A_k} \Big[(\mathbf{D}_p^k \, F_s \delta\mathbf{u}_s^k)^T (\mathbf{C}_{pp}^k \mathbf{D}_p^k \, F_\tau \mathbf{u}_\tau^k + \mathbf{C}_{pn}^k (\mathbf{D}_{n\Omega}^k + \mathbf{D}_{nz}^k) F_\tau \mathbf{u}_\tau^k)$$

$$+ ((\mathbf{D}_{n\Omega}^k + \mathbf{D}_{nz}^k) F_s \delta\mathbf{u}_s^k)^T (\mathbf{C}_{np}^k \mathbf{D}_p^k \, F_\tau \mathbf{u}_\tau^k + \mathbf{C}_{nn}^k (\mathbf{D}_{n\Omega}^k + \mathbf{D}_{nz}^k) F_\tau \mathbf{u}_\tau^k) \Big] d\Omega_k dz = \delta L_e^k \tag{34}$$

Applying now the formula of integration by parts, (34) becomes:

$$\int_{\Omega_k} \left((\mathbf{D}_\Omega) \delta\mathbf{a}^k \right)^T \mathbf{a}^k d\Omega_k = - \int_{\Omega_k} \delta\mathbf{a}^{k^T} \left((\mathbf{D}_\Omega^T) \mathbf{a}^k \right) d\Omega_k + \int_{\Gamma_k} \delta\mathbf{a}^{k^T} \left((\mathbf{I}_\Omega) \mathbf{a}^k \right) d\Gamma_k \tag{35}$$

where $\mathbf{I}_\Omega$ matrix is obtained applying the *Gradient theorem*:

$$\int_\Omega \frac{\partial\psi}{\partial x_i} dv = \oint_\Gamma n_i \psi ds \tag{36}$$

being n_i the components of the normal $\widehat{n}$ to the boundary along the direction i. After integration by parts, the governing equations and boundary conditions for the plate in the mechanical case are

obtained:

$$
\int_{\Omega_k} \int_{A_k} (\delta\mathbf{u}_s^k)^T \Big[\big((-\mathbf{D}_p^k)^T (\mathbf{C}_{pp}^k (\mathbf{D}_p^k) + \mathbf{C}_{pn}^k (\mathbf{D}_{n\Omega}^k + \mathbf{D}_{nz}^k) + (-\mathbf{D}_{n\Omega}^k + \mathbf{D}_{nz}^k)^T (\mathbf{C}_{np}^k (\mathbf{D}_p^k) + \mathbf{C}_{nn}^k (\mathbf{D}_{n\Omega}^k + \mathbf{D}_{nz}^k)) \big) \mathbf{F}_\tau \mathbf{F}_s \mathbf{u}_\tau^k \Big] dxdydz
$$

$$
+ \int_{\Omega_k} \int_{A_k} (\delta\mathbf{u}_s^k)^T \Big[\big(\mathbf{I}_p^{kT} (\mathbf{C}_{pp}^k (\mathbf{D}_p^k) + \mathbf{C}_{pn}^k (\mathbf{D}_{n\Omega}^k + \mathbf{D}_{nz}^k))
$$

$$
+ \mathbf{I}_{np}^{kT} (\mathbf{C}_{np}^k (\mathbf{D}_p^k) + \mathbf{C}_{nn}^k (\mathbf{D}_{n\Omega}^k + \mathbf{D}_{nz}^k)) \big) \mathbf{F}_\tau \mathbf{F}_s \mathbf{u}_\tau^k \Big] dxdydz = \int_{\Omega_k} \delta\mathbf{u}_s^{kT} F_s \mathbf{p}_u^k d\Omega_k \ . \qquad (37)
$$

where $\mathbf{I}_p^k$ and $\mathbf{I}_{np}^k$ depend on the boundary geometry:

$$
\mathbf{I}_p^k = \begin{bmatrix} n_x & 0 & 0 \\ 0 & n_y & 0 \\ n_y & n_x & 0 \end{bmatrix}, \quad \mathbf{I}_{np}^k = \begin{bmatrix} 0 & 0 & n_x \\ 0 & 0 & n_y \\ 0 & 0 & 0 \end{bmatrix} . \qquad (38)
$$

The normal to the boundary of domain Ω is:

$$
\widehat{\mathbf{n}} = \begin{bmatrix} n_x \\ n_y \end{bmatrix} = \begin{bmatrix} cos(\varphi_x) \\ cos(\varphi_y) \end{bmatrix} \qquad (39)
$$

where φ_x and φ_y are the angles between the normal $\widehat{n}$ and the direction x and y respectively.

5.6   Governing equations and boundary conditions

The governing equations for a multi-layered plate subjected to mechanical loadings are:

$$
\delta\mathbf{u}_s^{kT} : \qquad \mathbf{K}_{uu}^{k\tau s} \mathbf{u}_\tau^k = \mathbf{P}_{u\tau}^k \qquad (40)
$$

where the fundamental nucleus $\mathbf{K}_{uu}^{k\tau s}$ is obtained as:

$$
\mathbf{K}_{uu}^{k\tau s} = \Big[(-\mathbf{D}_p^k)^T (\mathbf{C}_{pp}^k (\mathbf{D}_p^k) + \mathbf{C}_{pn}^k (\mathbf{D}_{n\Omega}^k + \mathbf{D}_{nz}^k)
$$

$$
+ (-\mathbf{D}_{n\Omega}^k + \mathbf{D}_{nz}^k)^T (\mathbf{C}_{np}^k (\mathbf{D}_p^k) + \mathbf{C}_{nn}^k (\mathbf{D}_{n\Omega}^k + \mathbf{D}_{nz}^k)) \Big] \mathbf{F}_\tau \mathbf{F}_s \qquad (41)
$$

and the corresponding Neumann-type boundary conditions on Γ_k are:

$$
\mathbf{\Pi}_d^{k\tau s} \mathbf{u}_\tau^k = \mathbf{\Pi}_d^{k\tau s} \bar{\mathbf{u}}_\tau^k , \qquad (42)
$$

where:

$$\mathbf{\Pi}_d^{k\tau s} = \left[\mathbf{I}_p^{kT}(\mathbf{C}_{pp}^k(\mathbf{D}_p^k) + \mathbf{C}_{pn}^k(\mathbf{D}_{n\Omega}^k + \mathbf{D}_{nz}^k)) + \right.$$

$$\left. \mathbf{I}_{np}^{kT}(\mathbf{C}_{np}^k(\mathbf{D}_p^k) + \mathbf{C}_{nn}^k(\mathbf{D}_{n\Omega}^k + \mathbf{D}_{nz}^k))\right]\mathbf{F}_\tau \mathbf{F}_s \qquad (43)$$

and $\mathbf{P}_{u\tau}^k$ are variationally consistent loads with applied pressure.

For FG materials, the fundamental nuclei in explicit form becomes:

$$K_{uu_{11}}^{k\tau s} = (-\partial_x^\tau \partial_x^s C_{11} + \partial_z^\tau \partial_z^s C_{55} - \partial_y^\tau \partial_y^s C_{66})F_\tau F_s$$

$$K_{uu_{12}}^{k\tau s} = (-\partial_x^\tau \partial_y^s C_{12} - \partial_y^\tau \partial_x^s C_{66})F_\tau F_s$$
$$K_{uu_{13}}^{k\tau s} = (-\partial_x^\tau \partial_z^s C_{13} + \partial_z^\tau \partial_x^s C_{55})F_\tau F_s$$
$$K_{uu_{21}}^{k\tau s} = (-\partial_y^\tau \partial_x^s C_{12} - \partial_x^\tau \partial_y^s C_{66})F_\tau F_s$$
$$K_{uu_{22}}^{k\tau s} = (-\partial_y^\tau \partial_y^s C_{22} + \partial_z^\tau \partial_z^s C_{44} - \partial_x^\tau \partial_x^s C_{66})F_\tau F_s$$
$$K_{uu_{23}}^{k\tau s} = (-\partial_y^\tau \partial_z^s C_{23} + \partial_z^\tau \partial_y^s C_{44})F_\tau F_s$$
$$K_{uu_{31}}^{k\tau s} = (\partial_z^\tau \partial_x^s C_{13} - \partial_x^\tau \partial_z^s C_{55})F_\tau F_s$$
$$K_{uu_{32}}^{k\tau s} = (\partial_z^\tau \partial_y^s C_{23} - \partial_y^\tau \partial_z^s C_{44})F_\tau F_s$$
$$K_{uu_{33}}^{k\tau s} = (\partial_z^\tau \partial_z^s C_{33} - \partial_y^\tau \partial_y^s C_{44} - \partial_x^\tau \partial_x^s C_{55})F_\tau F_s$$
$$(44)$$

$$\Pi_{11}^{k\tau s} = (n_x \partial_x^s C_{11} + n_y \partial_y^s C_{66})F_\tau F_s$$

$$\Pi_{12}^{k\tau s} = (n_x \partial_y^s C_{12} + n_y \partial_x^s C_{66})F_\tau F_s$$
$$\Pi_{13}^{k\tau s} = (n_x \partial_z^s C_{13})F_\tau F_s$$
$$\Pi_{21}^{k\tau s} = (n_y \partial_x^s C_{12} + n_x \partial_y^s C_{66})F_\tau F_s$$
$$\Pi_{22}^{k\tau s} = (n_y \partial_y^s C_{22} + n_x \partial_x^s C_{66})F_\tau F_s$$
$$\Pi_{23}^{k\tau s} = (n_y \partial_z^s C_{23})F_\tau F_s$$
$$\Pi_{31}^{k\tau s} = (n_x \partial_z^s C_{55})F_\tau F_s$$
$$\Pi_{32}^{k\tau s} = (n_y \partial_z^s C_{44})F_\tau F_s$$
$$\Pi_{33}^{k\tau s} = (n_y \partial_y^s C_{44} + n_x \partial_x^s C_{55})F_\tau F_s \qquad (45)$$

5.7 Equations of motion and boundary conditions in terms of displacements

In order to discretize the linearized buckling equations by radial basis functions, we need the explicit terms of that equations and the corresponding boundary conditions as well in terms of the

generalized displacements. The explicit governing equations and corresponding boundary conditions in terms of generalized displacements for the static and free vibration analysis of functionally graded plates of the *sinus* theory can be found in [61]. Those equations are the same for the buckling problem, by setting to zero the terms with the inertias (I_i) as well as the external forces (p_z), and adding the non-linear terms to the δw_0 equation. For the sake of completeness we present here the equation of the buckling problem of *sinus* theory that corresponds to the w_0 variable.

$$
\begin{aligned}
\delta w_0 : \; & A_{13}\frac{\partial u_1}{\partial x} + 2B_{13}\frac{\partial u_Z}{\partial x} + A_{23}\frac{\partial v_1}{\partial y} + 2B_{23}\frac{\partial v_Z}{\partial y} - A_{55}\frac{\partial^2 w_0}{\partial x^2} - A_{44}\frac{\partial^2 w_0}{\partial y^2} \\
& -B_{55}\frac{\partial^2 w_1}{\partial x^2} - B_{44}\frac{\partial^2 w_1}{\partial y^2} - D_{55}\frac{\partial^2 w_Z}{\partial x^2} - D_{44}\frac{\partial^2 w_Z}{\partial y^2} \\
& +\bar{N}_{xx}\frac{\partial^2 w_0}{\partial x^2} + 2\bar{N}_{xy}\frac{\partial^2 w_0}{\partial x\partial y} + \bar{N}_{yy}\frac{\partial^2 w_0}{\partial y^2} = 0
\end{aligned}
\tag{46}
$$

The stiffness components of this equation can be computed as follows:

$$
A_{ij} = \sum_{k=1}^{N_l} C_{ij}^k \left(z_{k+1} - z_k\right); \quad B_{ij} = \frac{1}{2}\sum_{k=1}^{N_l} C_{ij}^k \left(z_{k+1}^2 - z_k^2\right); \quad D_{ij} = \frac{1}{3}\sum_{k=1}^{N_l} C_{ij}^k \left(z_{k+1}^3 - z_k^3\right)
\tag{47}
$$

where C_{ij}^k are the elastic constants previously defined in (28), (29), (31), and (32), N_l is the number of mathematical layers across the thickness direction, h_k is the thickness of each layer, and z_k, z_{k+1} are the lower and upper z coordinate for each layer k. $\bar{N}_{xx}$, $\bar{N}_{xy}$, and $\bar{N}_{yy}$ denote the in-plane applied loads.

6 The radial basis function method applied to buckling problems

Recently, radial basis functions (RBFs) have enjoyed considerable success and research as a technique for interpolating data and functions. A radial basis function, $\phi(\|x - x_j\|)$ is a spline that depends on the Euclidian distance between distinct data centers $x_j, j = 1, 2, ..., N \in \mathbb{R}^n$, also called nodal or collocation points. Although most work to date on RBFs relates to scattered data approximation and in general to interpolation theory, there has recently been an increased interest in their use for solving partial differential equations (PDEs). This approach, which approximates the whole solution of the PDE directly using RBFs, is truly a mesh-free technique. Kansa [75] introduced the concept of solving PDEs by an unsymmetric RBF collocation method based upon the

MQ interpolation functions, in which the shape parameter may vary across the problem domain.

The radial basis function (ϕ) approximation of a function (**u**) is given by

$$\widetilde{\mathbf{u}}(\mathbf{x}) = \sum_{i=1}^{N} \alpha_i \phi\left(\|x - y_i\|_2\right), \mathbf{x} \in \mathbb{R}^n \tag{48}$$

where $y_i, i = 1, .., N$ is a finite set of distinct points (centers) in $\mathbb{R}^n$.

Derivatives of **ũ** are computed as

$$\frac{\partial \widetilde{\mathbf{u}}}{\partial x} = \sum_{j=1}^{N} \alpha_j \frac{\partial \phi_j}{\partial x} \tag{49}$$

$$\frac{\partial^2 \widetilde{\mathbf{u}}}{\partial x^2} = \sum_{j=1}^{N} \alpha_j \frac{\partial^2 \phi_j}{\partial x^2}, \text{etc} \tag{50}$$

In the present collocation approach, one needs to impose essential and natural boundary conditions. Consider, for example, the condition $w = 0$, on a simply supported or clamped edge. The conditions are enforced by interpolating as

$$w = 0 \rightarrow \sum_{j=1}^{N} \alpha_j^W \phi_j = 0 \tag{51}$$

Other boundary conditions are interpolated in a similar way.

The most common RBFs are

$$\begin{aligned}
\text{Cubic:} \quad & \phi(r) = r^3 \\
\text{Thin plate splines:} \quad & \phi(r) = r^2 \log(r) \\
\text{Wendland functions:} \quad & \phi(r) = (1 - r)_+^m p(r) \\
\text{Gaussian:} \quad & \phi(r) = e^{-(cr)^2} \\
\text{Multiquadrics:} \quad & \phi(r) = \sqrt{c^2 + r^2} \\
\text{Inverse Multiquadrics:} \quad & \phi(r) = (c^2 + r^2)^{-1/2}
\end{aligned}$$

where the Euclidian distance r is real and non-negative and c is a positive shape parameter. In the present work, we consider the compact-support Wendland function [76] defined as

$$\phi(r) = (1 - c\,r)_+^8 \left(32(c\,r)^3 + 25(c\,r)^2 + 8c\,r + 1\right) \tag{52}$$

The shape parameter (c) is obtained by an optimization procedure, as detailed in Ferreira and Fasshauer [77].

Considering N distinct interpolations, and knowing $u(x_j)$, $j = 1, 2, ..., N$, one finds α_i by the solution of a $N \times N$ linear system

$$\mathbf{A}\alpha = \mathbf{u} \tag{53}$$

where $\mathbf{A} = [\phi\,(\|x - y_i\|_2)]_{N \times N}$, $\alpha = [\alpha_1, \alpha_2, ..., \alpha_N]^T$ and $\mathbf{u} = [u(x_1), u(x_2), ..., u(x_N)]^T$.

Consider a linear elliptic partial differential operator $\mathcal{L}$ acting in a bounded region Ω in $\mathbb{R}^n$ and another operator $\mathcal{L}_B$ acting on a boundary $\partial\Omega$. The eigenproblem looks for eigenvalues (λ) and eigenvectors ($\mathbf{u}$) that satisfy

$$\mathcal{L}\mathbf{u} + \lambda\mathbf{u} = 0 \text{ in } \Omega \tag{54}$$

$$\mathcal{L}_B\mathbf{u} = 0 \text{ on } \partial\Omega \tag{55}$$

The eigenproblem defined in (54) and (55) will be replaced by a finite-dimensional eigenvalue problem, after the radial basis approximations.

The solution of the eigenproblem by radial basis functions considers N_I nodes in the interior of the domain and N_B nodes on the boundary, with a total number of nodes $N = N_I + N_B$. In the present work, a $\mathfrak{R}^2$ Chebyshev grid is employed (see figure 6) and a square plate is computed with side length $a = 2$. For a given number of nodes per side ($N + 1$) they are generated by MATLAB code as:

```
x = cos(pi*(0:N)/N)'; y=x;
```

One advantage of such mesh is the concentration of points near the boundary.

The interpolation points are denoted by $x_i \in \Omega, i = 1, ..., N_I$ and $x_i \in \partial\Omega, i = N_I + 1, ..., N$. At the points in the domain, the following eigenproblem is defined

$$\sum_{i=1}^{N} \alpha_i \mathcal{L}\phi\,(\|x - y_i\|_2) = \lambda\widetilde{\mathbf{u}}(x_j), \ j = 1, 2, ..., N_I \tag{56}$$

or

$$\mathcal{L}^I\alpha = \lambda\widetilde{\mathbf{u}}^I \tag{57}$$

where

$$\mathcal{L}^I = \left[\mathcal{L}\phi \left(\|x - y_i\|_2 \right) \right]_{N_I \times N} \tag{58}$$

At the points on the boundary, the imposed boundary conditions are

$$\sum_{i=1}^{N} \alpha_i \mathcal{L}_B \phi \left(\|x - y_i\|_2 \right) = 0, \ j = N_I + 1, ..., N \tag{59}$$

or

$$\mathbf{B}\alpha = 0 \tag{60}$$

where $\mathbf{B} = \mathcal{L}_B \phi \left[\left(\|x_{N_I+1} - y_j\|_2 \right) \right]_{N_B \times N}$.

Therefore, one can write a finite-dimensional eigenvalue problem and solve equations (57) and (60) as a generalized eigenvalue problem

$$\begin{bmatrix} \mathcal{L}^I \\ \mathbf{B} \end{bmatrix} \alpha = \lambda \begin{bmatrix} \mathbf{A}^I \\ \mathbf{0} \end{bmatrix} \alpha \tag{61}$$

where

$$\mathbf{A}^I = \phi \left[\left(\|x_{N_I} - y_j\|_2 \right) \right]_{N_I \times N}$$

The eigenproblem associated to the linearized buckling equations is defined as

$$\left[\mathcal{L} - \lambda \mathcal{G} \right] \mathbf{X} = \mathbf{0} \tag{62}$$

where $\mathcal{L}$ collects all stiffness terms and $\mathcal{G}$ collects all terms related to the in-plane forces. In (62) $\mathbf{X}$ are the buckling modes associated with the buckling loads defined as λ.

7 Numerical results

In this section the sinusoidal shear deformation plate theories are combined with radial basis functions collocation for the buckling analysis of functionally graded sandwich plates. The plate is subjected to compressive in-plane forces acting on the mid-plane of the plate. The buckling loads of simply supported (SSSS) square ($a = b = 2$, see figure 6) sandwich plates with FG materials in

the skins are analysed, for both symmetric and unsymmetric plates. The plates have side lengths $a = b$, thickness h, being the span-to-thickness ratio a/h taken to be 10.

As stated before, all numerical examples are performed employing a Chebyshev grid and the Wendland function as defined in (52) with an optimized shape parameter. The bottom skin varies from a metal-rich surface to a ceramic-rich surface while the top skin face varies from a ceramic-rich surface to a metal-rich surface. The core material of the present sandwich plate is fully ceramic. Recall that the plate is a sandwich, physicaly divided into 3 layers, although 91 virtual layers are considered for the evaluation of stiffness components. The power-law function is used to describe the volume fraction of the metal and ceramic phases (see (1)) and the material homogeneization technique adopted is the law of mixtures (16), the same used in the references. The material properties are $E_m = 70E_0$ (aluminum) and $E_c = 380E_0$ (alumina) being $E_0 = 1$GPa. Poisson's ratio is $\nu_m = \nu_c = \nu = 0.3$ for both aluminum and alumina. The homogeneization technique is applied to the Young's modulus only. Various power-law exponents, and skin-core-skin thickness ratios are considered in the following.

Both the uni- and bi-axial critical buckling load are studied. An initial study was performed for each type of buckling load to show the convergence of the present approach and select the number of Chebyshev points to use in the computation of the buckling problems. The non-dimensional parameter used is

$$\bar{P} = \frac{Pa^2}{100h^3 E_0}.$$

7.1 Uni-axial buckling load

The uni-axial case convergence study is presented in table 2 for the 1-1-1 sandwich with $p = 1$. Based on this study a grid of 17^2 points was used for the forward uni-axial buckling study.

The first four buckling modes of a simply supported 2-2-1 sandwich square plate with FG skins, $p = 10$, subjected to a uni-axial in-plane compressive load, using present sinusoidal theories are presented in figures 7 to 10.

The critical buckling loads obtained from the present approach with *sinus*, *sinus*0, *sinusZZ*, and *sinusZZ*0 theories are tabulated and compared with available references in table 3 for various power-law exponents p and skin-core-skin thickness ratios. The table includes results obtained from classical plate theory (CLPT), first-order shear deformation plate theory (FSDPT, $K = 5/6$

as shear correction factor), Reddy's third-order shear deformation plate theory (TSDPT) [10], and Zenkour's sinusoidal shear deformation plate theory (SSDPT) [29]. The table is organized so that the material power-law exponent increases from up to down (p = 0, 0.5, 1, 5, 10) and the core thickness to the total thickness of the plate ratio increases from left to right $\left(\frac{h_c}{h} = 0, \frac{1}{5}, \frac{1}{4}, \frac{1}{3}, \frac{2}{5}, \frac{1}{2}\right)$. In the particular case of the 1-0-1 sandwich, the sandwich degenerates in a FG two layers plate (see figure 11 on the left) and the ZZF is as in figure 11 on the right.

7.2   Bi-axial buckling load

The bi-axial case convergence study is presented in table 4 for the 2-1-1 sandwich with p = 5. A grid of 17^2 points was used for the forward bi-axial buckling study.

In figures 12 to 15 the first four buckling modes of a simply supported 2-1-2 sandwich square plate with FG skins, p = 0.5, subjected to a bi-axial in-plane compressive load, using present sinusoidal theories are presented.

The critical buckling loads obtained from the present approach with *sinus*, *sinus*0, *sinusZZ*, and *sinusZZ*0 theories are tabulated in table 5 for various power-law exponents p and skin-core-skin thickness ratios. As for the uni-axial case, results are compared with those from classical plate theory (CLPT), first-order shear deformation plate theory (FSDPT, K = 5/6 as shear correction factor), Reddy's third-order shear deformation plate theory (TSDPT) [10], and Zenkour's sinusoidal shear deformation plate theory (SSDPT) [29]. The table is organized so that the material power-law exponent increases from up to down and the core thickness to the total thickness of the plate ratio increases from left to right. As in the uni-axial load case, the 1-0-1 case becomes as in figure 11.

7.3   Discussion of results

Results obtained with the present formulation are in good agreement with considered references (except for the classical plate theory, which is not adequate for this type of plates). This allow us to conclude that the sinusoidal plate theories combined with collocation with radial basis functions are good for the modeling of SSSS sandwich plates with FG skins.

The isotropic fully ceramic plate (first line on tables 3 and 5) has the higher fundamental buckling

loads. As the core thickness to the total thickness of the plate ratio increases the buckling loads increase as well. We may also conclude that the critical buckling loads decrease as the power-law exponent p increases. From the comparison of tables 3 and 5 we deduce that the bi-axial buckling load of any simply supported sandwich square plate with FG skins is half the uni-axial one for the same plate.

The zig-zag effects have influence on the buckling loads of SSSS sandwich plates with functionally graded skins. By comparing *sinus* and *sinus*ZZ theories we see that the first one (without ZZ effect) gives higher buckling loads than the other (with ZZ effects). Same happens to *sinus*0 and *sinus*ZZ0 theories. The influence of the ZZ effect is also seen in the first column of tables 3 and 5: for the isotropic fully ceramic plate, different values are obtained.

Another thing to note is that the *sinus*0 and *sinus*ZZ0 theories are in better agreement with [10] and [29] than *sinus* and *sinus*ZZ theories. This can be explained by the $\epsilon_{zz} = 0$ option that the four theories *sinus*0, *sinus*ZZ0, [10] and [29] share. The influence of the warping effects is stronger than the ZZ effects.

8   Conclusions

For the first time, a study on the influence of Zig-Zag and warping effects on buckling problems of functionally graded sandwich plates by radial basis function collocation was performed. For that purpose, four sinusoidal theories were compared. The computation procedure becomes fast and straightforward in MATLAB as a consequence of combining a generalized version of Carrera's Unified Formulation and collocation with radial basis functions. The collocation code depends only on the choice of two vectors and the buckling loads for any type of C_z^0 shear deformation theory are obtained just by changing F_τ and F_s. The present formulation was compared with available references and proved very accurate in buckling problems.

Although buckling loads of sandwich plates with functionally graded skins depend on both warping and zig-zag effects, the influence of the warping effects is stronger.

References

[1] M.B. Bever and P.E. Duwez. Gradients in composite materials. *Materials Science and Engineering*, 10(0):1 – 8, 1972.

[2] Y. Miyamoto, W.A. Kaysser, B.H. Rabin, A. Kawasaki, and R.G. Ford. *Functionally Graded Materials: Design, Processing and Applications*. Kluwer Academic Publishers, 1999.

[3] F.J. Ferrante and L.L. Graham-Brady. Stochastic simulation of non-gaussian/non-stationary properties in a functionally graded plate. *Computer Methods in Applied Mechanics and Engineering*, 194(12-16):1675 – 1692, 2005.

[4] H.M Yin, L.Z Sun, and G.H Paulino. Micromechanics-based elastic model for functionally graded materials with particle interactions. *Acta Materialia*, 52(12):3535 – 3543, 2004.

[5] Zheng Zhong and Ertao Shang. Closed-form solutions of three-dimensional functionally graded plates. *Mechanics of Advanced Materials and Structures*, 15(5):355–363, 2008.

[6] T. K. Nguyen, K. Sab, and G. Bonnet. Shear correction factors for functionally graded plates. *Mechanics of Advanced Materials and Structures*, 14(8):567–575, 2007.

[7] Victor Birman and Larry W. Byrd. Modeling and analysis of functionally graded materials and structures. *Applied Mechanics Reviews*, 60(5):195–216, 2007.

[8] M. Koizumi. Fgm activities in japan. *Composites Part B: Engineering*, 28(1-2):1 – 4, 1997. Use of Composites Multi-Phased and Functionally Graded Materials.

[9] J. N. Reddy and C. D. Chin. Thermomechanical analysis of functionally graded cylinders and plates. *Journal of Thermal Stresses*, 21(6):593–626, 1998.

[10] J. N. Reddy. Analysis of functionally graded plates. *International Journal for Numerical Methods in Engineering*, 47:663–684, 2000.

[11] S. S. Vel and R. C. Batra. Three-dimensional analysis of transient thermal stresses in functionally-graded plates. *International Journal of Solids and Structures*, in press, 2003.

[12] S. S. Vel and R. C. Batra. Exact solution for thermoelastic deformations of functionally graded thick rectangular plates. *AIAA Journal*, 40:1421–1433, 2002.

[13] Z. Q. Cheng and R. C. Batra. Three-dimensional thermoelastic deformations of a functionally graded-elliptic plate. *Composites: Part B*, 31:97–106, 2000.

[14] Javaheri R. and Eslami M. R. Thermal buckling of functionally graded plates based on higher order theory. *Journal of Thermal Stresses*, 25(7):603–625, 2002.

[15] M. Kashtalyan. Three-dimensional elasticity solution for bending of functionally graded rectangular plates. *European Journal of Mechanics - A/Solids*, 23(5):853 – 864, 2004.

[16] M. Kashtalyan and M. Menshykova. Three-dimensional elasticity solution for sandwich panels with a functionally graded core. *Composite Structures*, 87(1):36 – 43, 2009.

[17] L. F. Qian, R. C. Batra, and L. M. Chen. Static and dynamic deformations of thick functionally graded elastic plate by using higher-order shear and normal deformable plate theory and meshless local petrov-galerkin method. *Composites: Part B*, 35:685–697, 2004.

[18] A.M. Zenkour. A comprehensive analysis of functionally graded sandwich plates: Part 1–deflection and stresses. *International Journal of Solids and Structures*, 42(18-19):5224 – 5242, 2005.

[19] A. M. Zenkour. Generalized shear deformation theory for bending analysis of functionally graded plates. *Appl Math Modell*, 30:67–84, 2006.

[20] Fernando Ramirez, Paul R. Heyliger, and Ernian Pan. Static analysis of functionally graded elastic anisotropic plates using a discrete layer approach. *Composites Part B: Engineering*, 37(1):10 – 20, 2006.

[21] A. J. M. Ferreira, R. C. Batra, C. M. C. Roque, L. F. Qian, and P. A. L. S. Martins. Static analysis of functionally graded plates using third-order shear deformation theory and a meshless method. *Composite Structures*, 69(4):449–457, 2005.

[22] A. J. M. Ferreira, C. M. C. Roque, R. M. N. Jorge, G. E. Fasshauer, and R. C. Batra. Analysis of functionally graded plates by a robust meshless method. *Mechanics of Advanced Materials and Structures*, 14(8):577–587, 2007.

[23] Shyang-Ho Chi and Yen-Ling Chung. Mechanical behavior of functionally graded material plates under transverse load–part i: Analysis. *International Journal of Solids and Structures*, 43(13):3657 – 3674, 2006.

[24] Shyang-Ho Chi and Yen-Ling Chung. Mechanical behavior of functionally graded material plates under transverse load–part ii: Numerical results. *International Journal of Solids and Structures*, 43(13):3675 – 3691, 2006.

[25] Z. Q. Cheng and R. C. Batra. Deflection relationships between the homogeneous kirchhoff plate theory and different functionally graded plate theories. *Archive of Mechanics*, 52:143–158, 2000.

[26] R.C. Batra and J. Jin. Natural frequencies of a functionally graded anisotropic rectangular plate. *Journal of Sound and Vibration*, 282(1-2):509 – 516, 2005.

[27] A. J. M. Ferreira, R. C. Batra, C. M. C. Roque, L. F. Qian, and R. M. N. Jorge. Natural frequencies of functionally graded plates by a meshless method. *Composite Structures*, 75(1-4):593–600, September 2006.

[28] S. S. Vel and R. C. Batra. Three-dimensional exact solution for the vibration of functionally graded rectangular plates. *Journal of Sound and Vibration*, 272:703–730, 2004.

[29] A.M. Zenkour. A comprehensive analysis of functionally graded sandwich plates: Part 2–buckling and free vibration. *International Journal of Solids and Structures*, 42(18-19):5243 – 5258, 2005.

[30] C.M.C. Roque, A.J.M. Ferreira, and R.M.N. Jorge. A radial basis function approach for the free vibration analysis of functionally graded plates using a refined theory. *Journal of Sound and Vibration*, 300(3-5):1048 – 1070, 2007.

[31] Z. Q. Cheng and R. C. Batra. Exact correspondence between eigenvalues of membranes and functionally graded simply supported polygonal plates. *Journal of Sound and Vibration*, 229:879–895, 2000.

[32] M. M. Najafizadeh and M. R. Eslami. Buckling analysis of circular plates of functionally graded materials under uniform radial compression. *International Journal of Mechanical Sciences*, 44(12):2479 – 2493, 2002.

[33] V. Birman. Buckling of functionally graded hybrid composite plates. *Proceedings of the 10th Conference on Engineering Mechanics*, pages 1199–1202, 1995.

[34] R. Javaheri and M.R. Eslami. Buckling of functionally graded plates under in-plane compressive loading. *ZAMM - Journal of Applied Mathematics and Mechanics / Zeitschrift fÃijr Angewandte Mathematik und Mechanik*, 82(4):277–283, 2002.

[35] E. Carrera, S. Brischetto, M. Cinefra, and M. Soave. Effects of thickness stretching in functionally graded plates and shells. *Composites Part B: Engineering*, 42:123–133, 2011.

[36] G. Kirchhoff. Uber das gleichgewicht und die bewegung einer elastischen scheibe. *J. Angew. Math.*, 40:51–88, 1850.

[37] E. Reissner. The effect of transverse shear deformations on the bending of elastic plates. *Journal of Applied mechanics*, 12:A69–A77, 1945.

[38] R. D. Mindlin. Influence of rotary inertia and shear in flexural motions of isotropic elastic plates. *Journal of Applied mechanics*, 18:31–38, 1951.

[39] S. Burton and A. K. Noor. Assessment of computational model for sandwich panels and shells. *Comput. Meth. Appl. Mech. Eng.*, 124:125–151, 1995.

[40] A. K. Noor, S. Burton, and C. W. Bert. Computational model for sandwich panels and shells. *Appl. Mech. Rev.*, 49:155–199, 1996.

[41] H. Altenbach. Theories for laminated and sandwich plates. *Mechanics of Composite Materials*, 34:243–252, 1998. 10.1007/BF02256043.

[42] Liviu Librescu and Terry Hause. Recent developments in the modeling and behavior of advanced sandwich constructions: a survey. *Composite Structures*, 48(1-3):1 – 17, 2000.

[43] Jack R. Vinson. Sandwich structures. *Applied Mechanics Reviews*, 54(3):201–214, 2001.

[44] L. Demasi. 2d, quasi 3d and 3d exact solutions for bending of thick and thin sandwich plates. *J. Sandwich Struct. Mater.*, 10:271–310, 2008.

[45] E. Carrera. Historical review of zig-zag theories for multilayered plates and shells. *Applied Mechanics Reviews*, (56):287–308, 2003.

[46] H. Murakami. Laminated composite plate theory with improved in-plane responses. *Journal of Applied Mechanics*, 53:661–666, 1986.

[47] E. Carrera. Developments, ideas, and evaluations based upon reissner's mixed variational theorem in the modelling of multilayered plates and shells. *Applied Mechanics Reviews*, 54:301–329, 2001.

[48] E. Carrera. The use of murakami's zig-zag function in the modeling of layered plates and shells. *Compos. Struct.*, 82:541–554, 2004.

[49] L. Demasi. ∞^3 hierarchy plate theories for thick and thin composite plates: the generalized unified formulation. *Compos. Struct.*, 84:256–270, 2008.

[50] S. Brischetto, E. Carrera, and L. Demasi. Improved bending analysis of sandwich plate by using zig-zag function. *Compos. Struct.*, 89:408–415, 2009.

[51] E. Carrera. C^0 reissner-mindlin multilayered plate elements including zig-zag and interlaminar stress continuity. *International Journal of Numerical Methods in Engineering*, 39:1797–1820, 1996.

[52] A. J. M. Ferreira. A formulation of the multiquadric radial basis function method for the analysis of laminated composite plates. *Composite Structures*, 59:385–392, 2003.

[53] A. J. M. Ferreira. Thick composite beam analysis using a global meshless approximation based on radial basis functions. *Mechanics of Advanced Materials and Structures*, 10:271–284, 2003.

[54] A. J. M. Ferreira, C. M. C. Roque, and P. A. L. S. Martins. Analysis of composite plates using higher-order shear deformation theory and a finite point formulation based on the multiquadric radial basis function method. *Composites: Part B*, 34:627–636, 2003.

[55] A.J.M. Ferreira, C.M.C. Roque, R.M.N. Jorge, and E.J. Kansa. Static deformations and vibration analysis of composite and sandwich plates using a layerwise theory and multiquadrics discretizations. *Engineering Analysis with Boundary Elements*, 29(12):1104 – 1114, 2005.

[56] A.J.M. Ferreira, C.M.C. Roque, and R.M.N. Jorge. Analysis of composite plates by trigonometric shear deformation theory and multiquadrics. *Computers & Structures*, 83(27):2225 – 2237, 2005.

[57] A.J.M. Ferreira, R.C. Batra, C.M.C. Roque, L.F. Qian, and R.M.N. Jorge. Natural frequencies of functionally graded plates by a meshless method. *Composite Structures*, 75(1-4):593 – 600, 2006. Thirteenth International Conference on Composite Structures - ICCS/13.

[58] A.J.M. Ferreira, C.M.C. Roque, and R.M.N. Jorge. Free vibration analysis of symmetric laminated composite plates by fsdt and radial basis functions. *Computer Methods in Applied Mechanics and Engineering*, 194(39-41):4265 – 4278, 2005.

[59] A. J. M. Ferreira, C. M. C. Roque, and P. A. L. S. Martins. Radial basis functions and higher-order shear deformation theories in the analysis of laminated composite beams and plates. *Composite Structures*, 66(1-4):287 – 293, 2004. Twelfth International Conference on Composite Structures.

[60] A.M.A. Neves, A.J.M. Ferreira, E. Carrera, C.M.C. Roque, M. Cinefra, R.M.N. Jorge, and C.M.M. Soares. Bending of fgm plates by a sinusoidal plate formulation and collocation with radial basis functions. *Mechanics Research Communications*, 38(5):368 – 371, 2011.

[61] A.M.A. Neves, A.J.M. Ferreira, E. Carrera, C.M.C. Roque, M. Cinefra, R.M.N. Jorge, and C.M.M. Soares. A quasi-3d sinusoidal shear deformation theory for the static and free vibration analysis of functionally graded plates. *Composites Part B: Engineering*, 43:711–725, 2012.

[62] A.J.M. Ferreira, C.M.C. Roque, E. Carrera, M. Cinefra, and O. Polit. Radial basis functions collocation and a unified formulation for bending, vibration and buckling analysis of laminated plates, according to a variation of murakami's zig-zag theory. *European Journal of Mechanics - A/Solids*, 30(4):559 – 570, 2011.

[63] J.D. Rodrigues, C.M.C. Roque, A.J.M. Ferreira, E. Carrera, and M. Cinefra. Radial basis functions-finite differences collocation and a unified formulation for bending, vibration and buckling analysis of laminated plates, according to murakami's zig-zag theory. *Composite Structures*, 93(7):1613 – 1620, 2011.

[64] A.J.M. Ferreira, C.M.C. Roque, E. Carrera, M. Cinefra, and O. Polit. Two higher order zig-zag theories for the accurate analysis of bending, vibration and buckling response of laminated plates by radial basis functions collocation and a unified formulation. *Journal of Composite Materials*, 45(24):2523–2536, 2011.

[65] M. Touratier. A generalization of shear deformation theories for axisymmetric multilayered shells. *International Journal of Solids and Structures*, 29:1379–1399, 1992.

[66] M. Touratier. An efficient standard plate theory. *International Journal of Engineering Science*, 29:901–916, 1991.

[67] M. Touratier. A refined theory of laminated shallow shells. *International Journal of Solids and Structures*, 29(11):1401–1415, 1992.

[68] P. Vidal and O. Polit. A family of sinus finite elements for the analysis of rectangular laminated beams. *Composite Structures*, 84:56–72, 2008.

[69] A. M. A. Neves, A. J. M. Ferreira, E. Carrera, M. Cinefra, R. M. N. Jorge, and C. M. M. Soares. Static analysis of functionally graded sandwich plates according to a hyperbolic theory considering zig-zag and warping effects. *Advances in Engineering Software*, 52:30–43, 2012.

[70] Z. H. Jin and R. C. Batra. Stress intensity relaxation at the tip of an edge crack in a functionally graded material subjected to a thermal shock. *Journal of Thermal Stresses*, 19:317–339, 1996.

[71] Y.L. Chung and S.H. Chi. The residual stress of functionally graded materials. *Journal of the Chinese Institute of Civil and Hydraulic Engineering*, 13:1–9, 2001.

[72] G. N. Praveen and J. N. Reddy. Nonlinear transient thermoelastic analysis of functionally graded ceramic-metal plates. *International Journal of Solids and Structures*, 35(33):4457 – 4476, 1998.

[73] T Mori and K Tanaka. Average stress in matrix and average elastic energy of materials with misfitting inclusions. *Acta Metallurgica*, 21(5):571 – 574, 1973.

[74] Y. and Benveniste. A new approach to the application of mori-tanaka's theory in composite materials. *Mechanics of Materials*, 6(2):147 – 157, 1987.

[75] E. J. Kansa. Multiquadrics- a scattered data approximation scheme with applications to computational fluid dynamics. i: Surface approximations and partial derivative estimates. *Computers and Mathematics with Applications*, 19(8/9):127–145, 1990.

[76] H. Wendland. Error estimates for interpolation by compactly supported radial basis functions of minimal degree. *J. Approx. Theory*, 93:258–296, 1998.

[77] A. J. M. Ferreira and G. E. Fasshauer. Computation of natural frequencies of shear deformable beams and plates by a rbf-pseudospectral method. *Computer Methods in Applied Mechanics and Engineering*, 196:134–146, 2006.

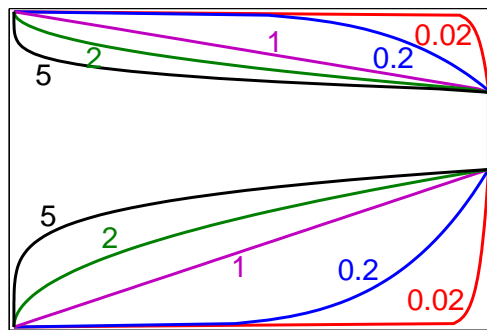Fig. 1. Sandwich with isotropic core and FG skins.

Fig. 2. A 2-1-1 sandwich with FG skins for various power-law exponents in (1).
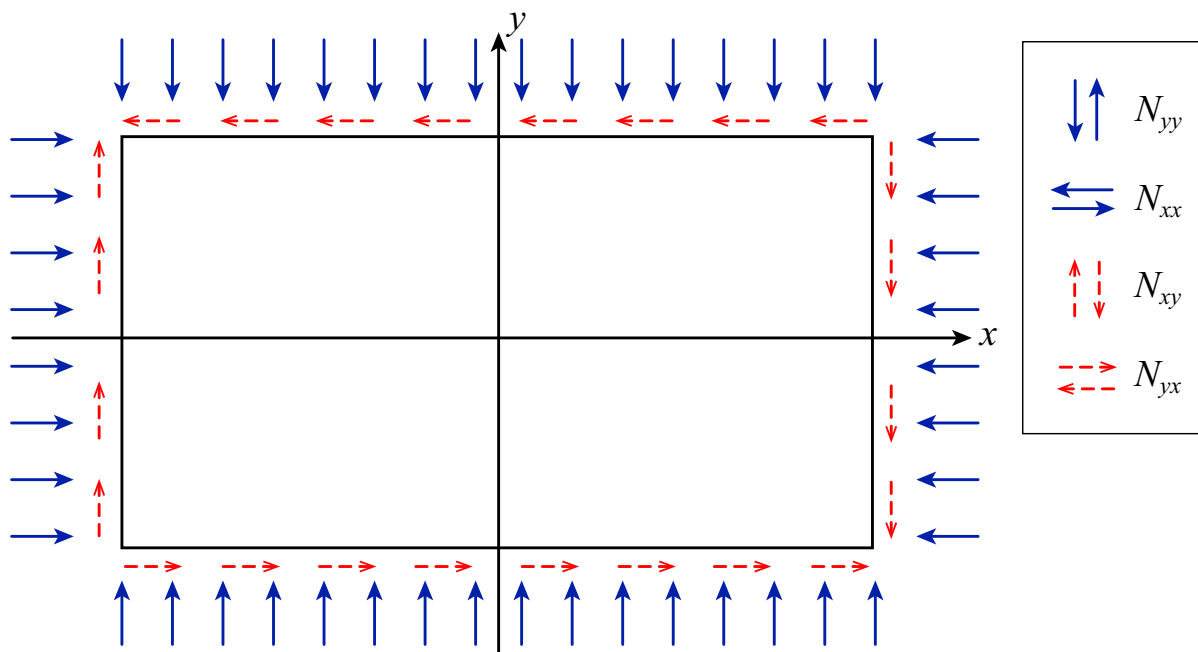
Fig. 3. Rectangular plate subjected to in-plane forces.
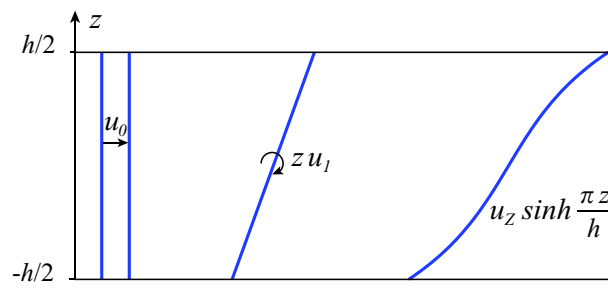
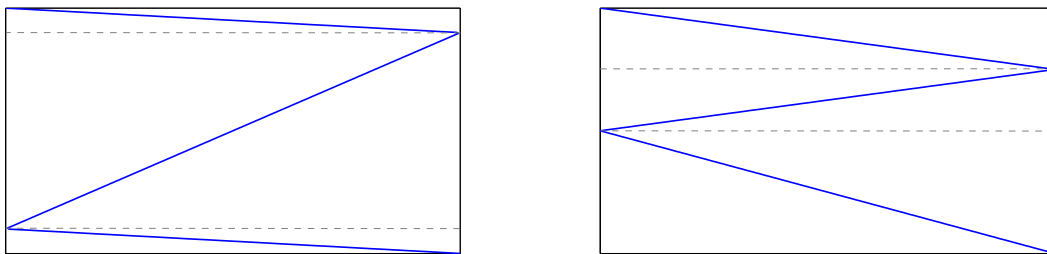Fig. 4. Scheme of the expansions involved in the displacement field.

Fig. 5. Zig-Zag effect for the 1-8-1 (left) and the 2-1-1 sandwiches (right).

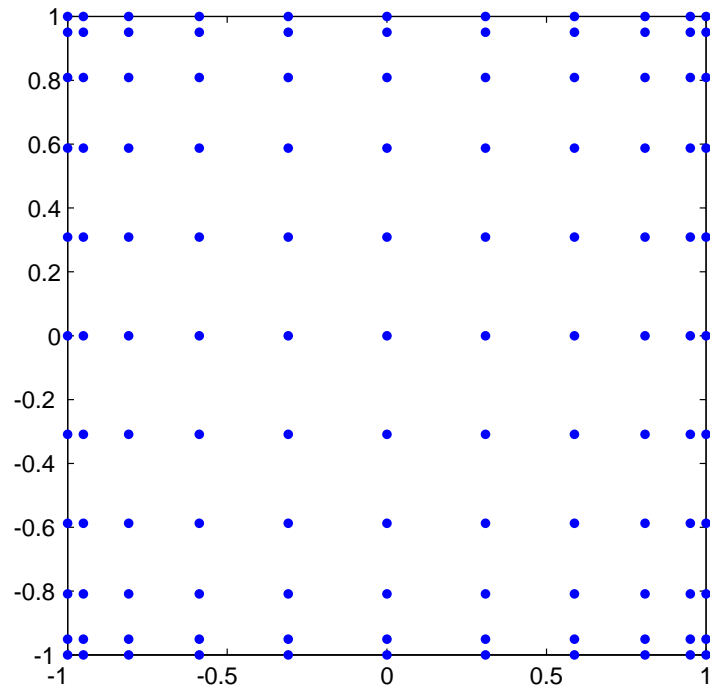Fig. 6. A sketch of a $\mathfrak{R}^2$ Chebyshev grid with 11^2 points

Fig. 7. First four buckling modes. Uni-axial buckling load of a simply supported 2-2-1 sandwich square plate with FG skins, $p = 10$, and using the sinus theory.

Fig. 8. First four buckling modes. Uni-axial buckling load of a simply supported 2-2-1 sandwich square plate with FG skins, $p = 10$, and using the sinus0 theory.

eig = 3.660001201833   eig = 5.503702635590

eig = 9.206522130807   eig = 13.578579962283

Fig. 9. First four buckling modes. Uni-axial buckling load of a simply supported 2-2-1 sandwich square plate with FG skins, $p = 10$, and using the sinusZZ theory.

eig = 3.670154303668   eig = 5.540913251794

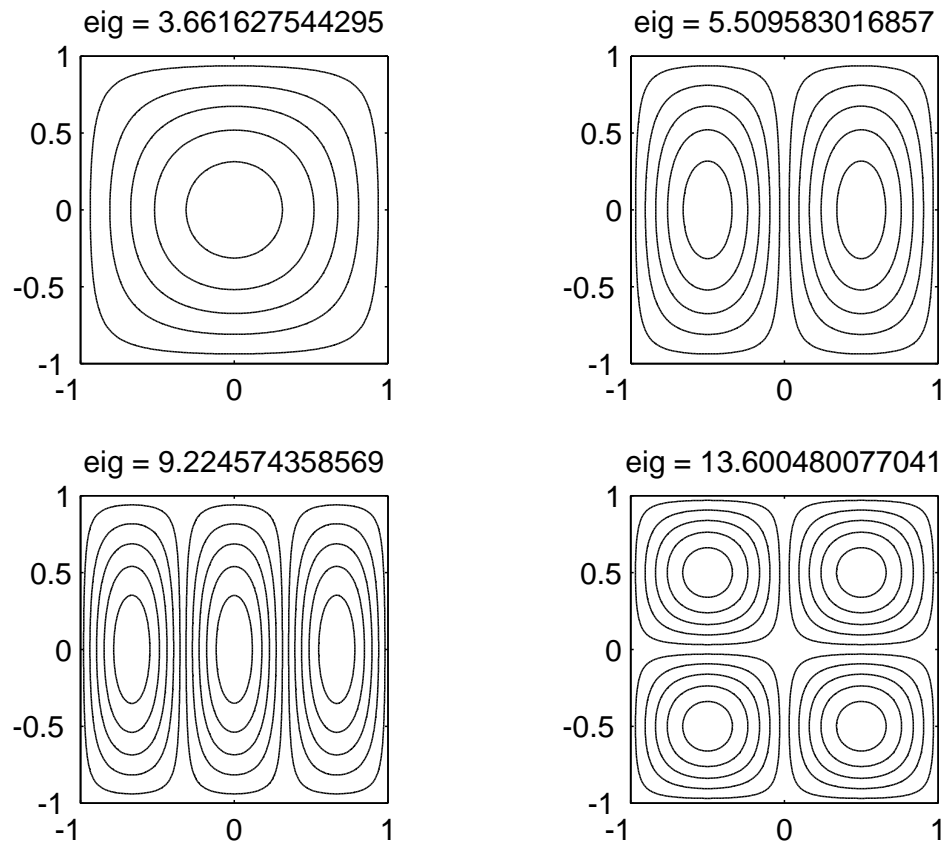eig = 9.325969618823   eig = 13.721717248356

Fig. 10. First four buckling modes. Uni-axial buckling load of a simply supported 2-2-1 sandwich square plate with FG skins, $p = 10$, and using the sinusZZ0 theory.
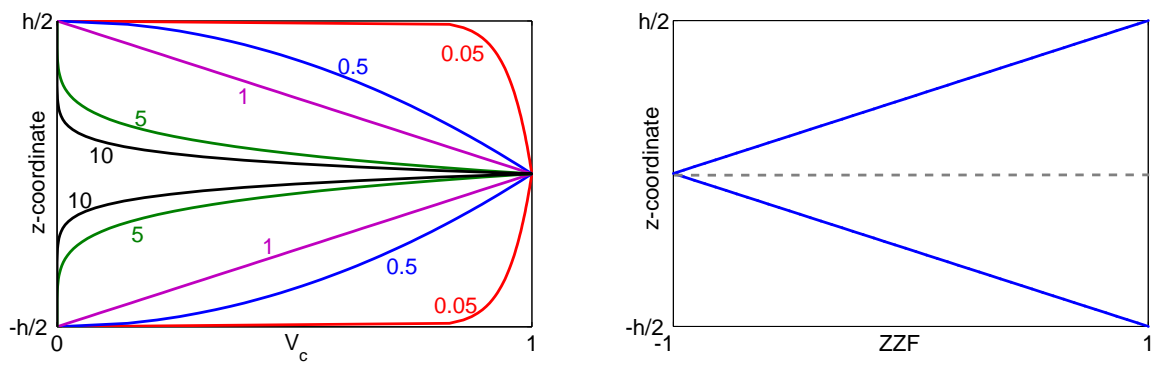
Fig. 11. The 1-0-1 sandwich with FG skins: influence of the exponent power-law (left) and the ZZF (right).

eig = 3.858210415448

eig = 9.087836102889

eig = 9.087836208572

eig = 13.745581299390
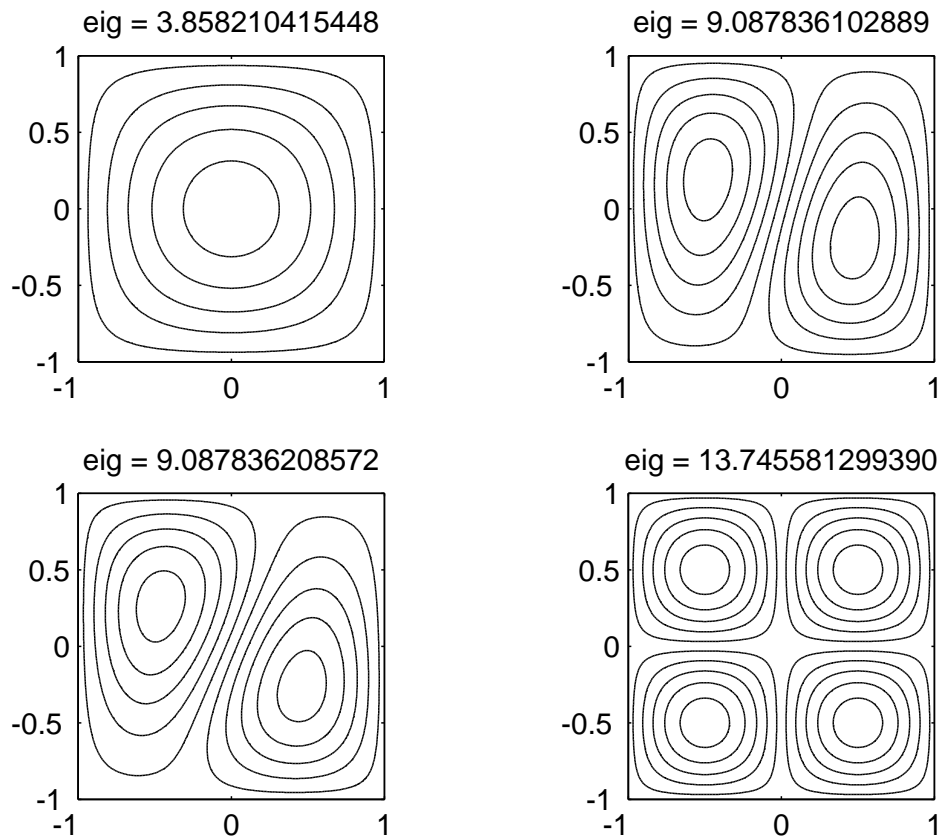
Fig. 12. First four buckling modes. Bi-axial buckling load of a simply supported 2-1-2 sandwich square plate with FG skins, $p = 0.5$, and using the sinus theory.
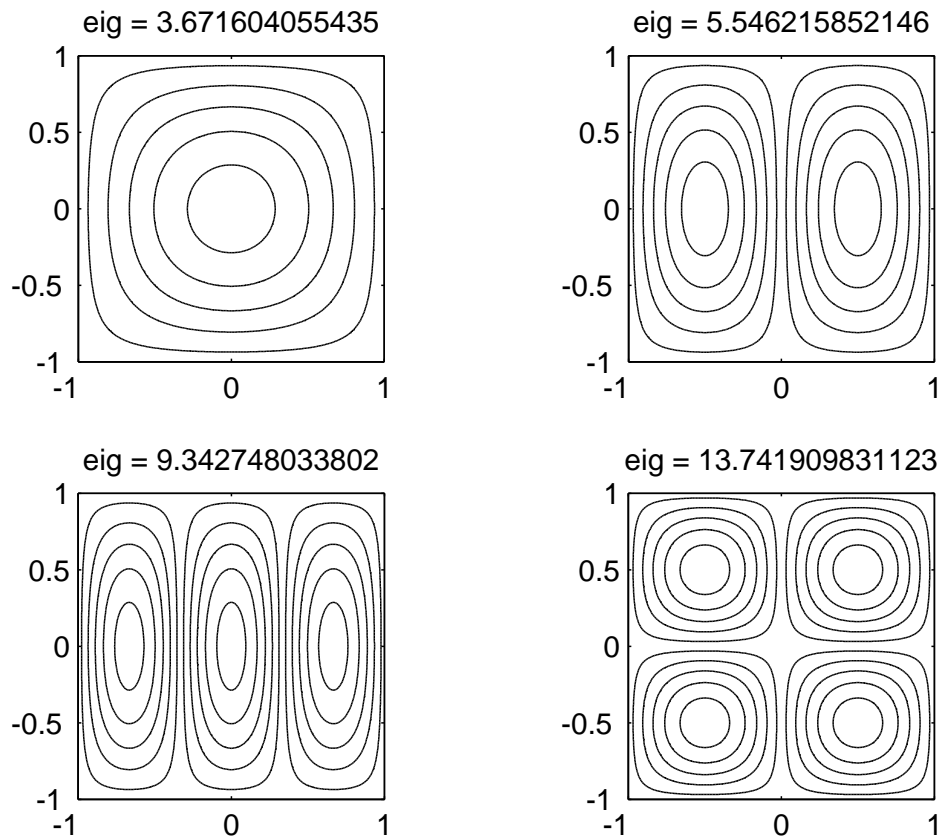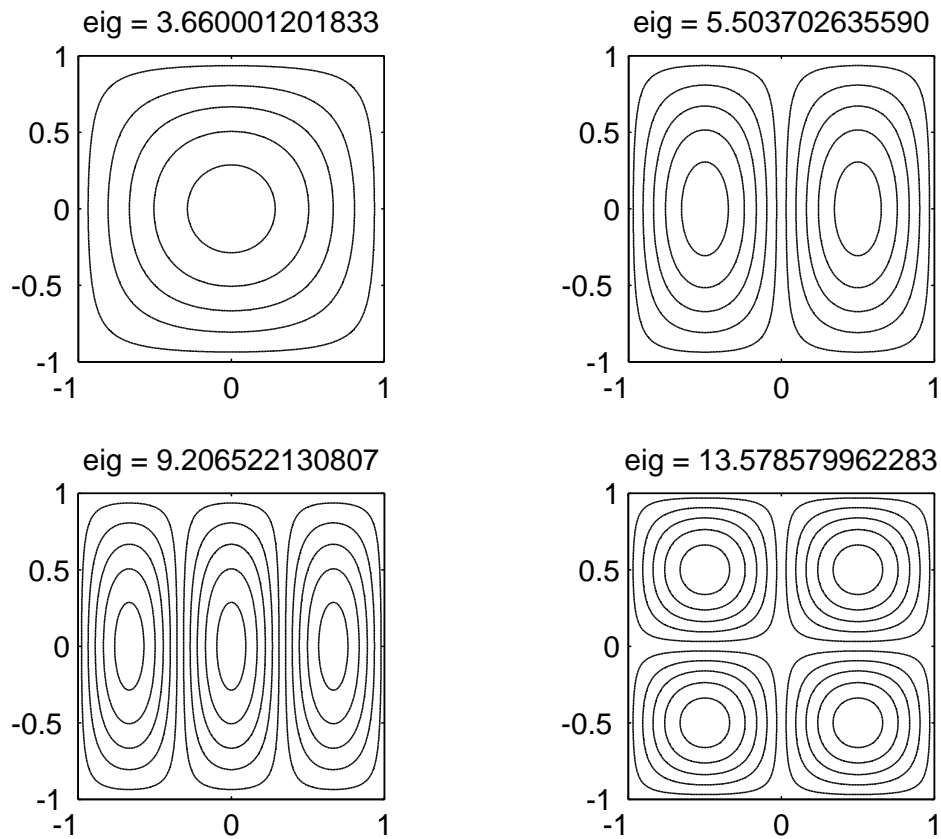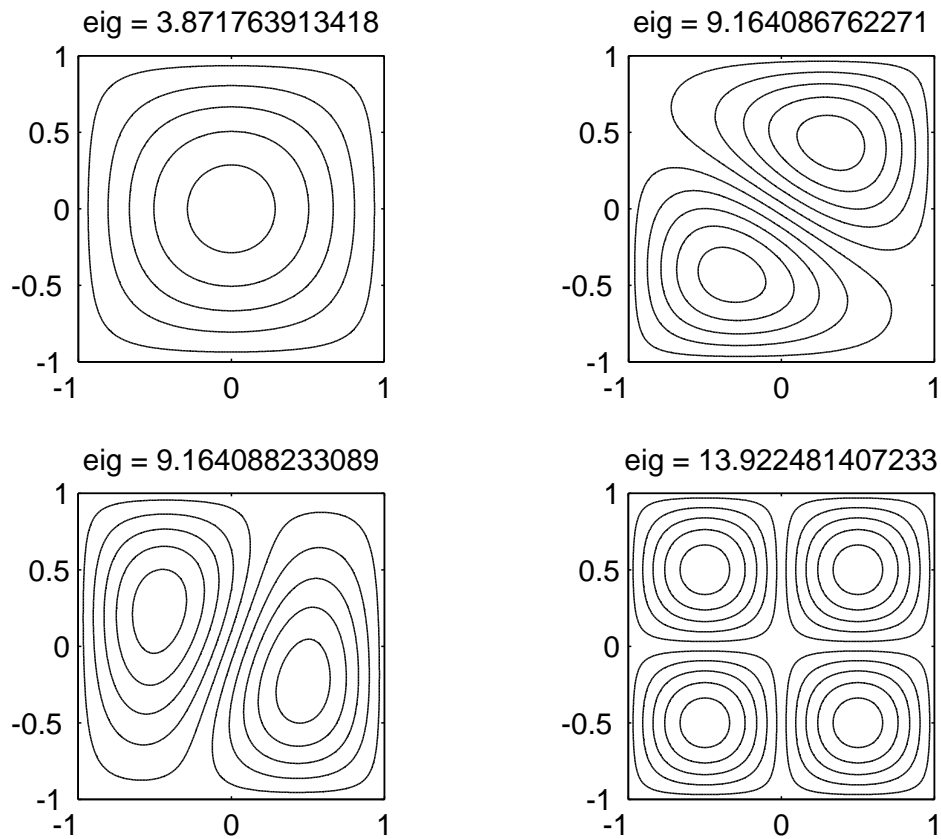
Fig. 13. First four buckling modes. Bi-axial buckling load of a simply supported 2-1-2 sandwich square plate with FG skins, $p = 0.5$, and using the sinus0 theory.

Fig. 14. First four buckling modes. Bi-axial buckling load of a simply supported 2-1-2 sandwich square plate with FG skins, $p = 0.5$, and using the sinusZZ theory.

eig = 3.871548426992

eig = 9.162892533640

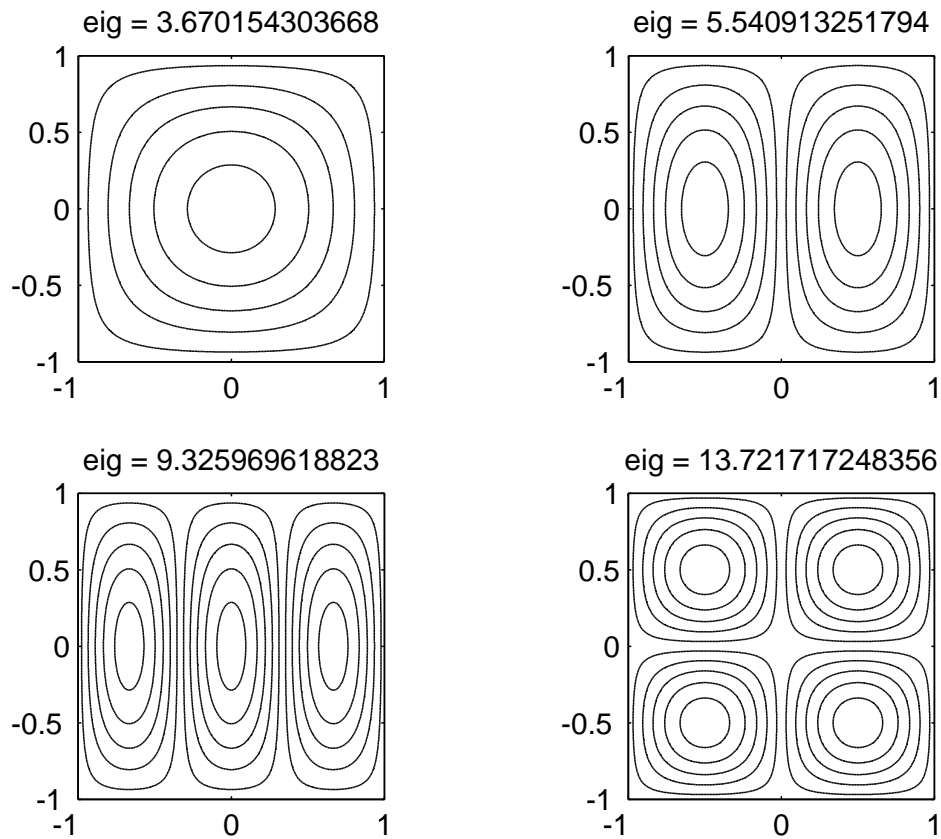eig = 9.162894344268

eig = 13.919866759501
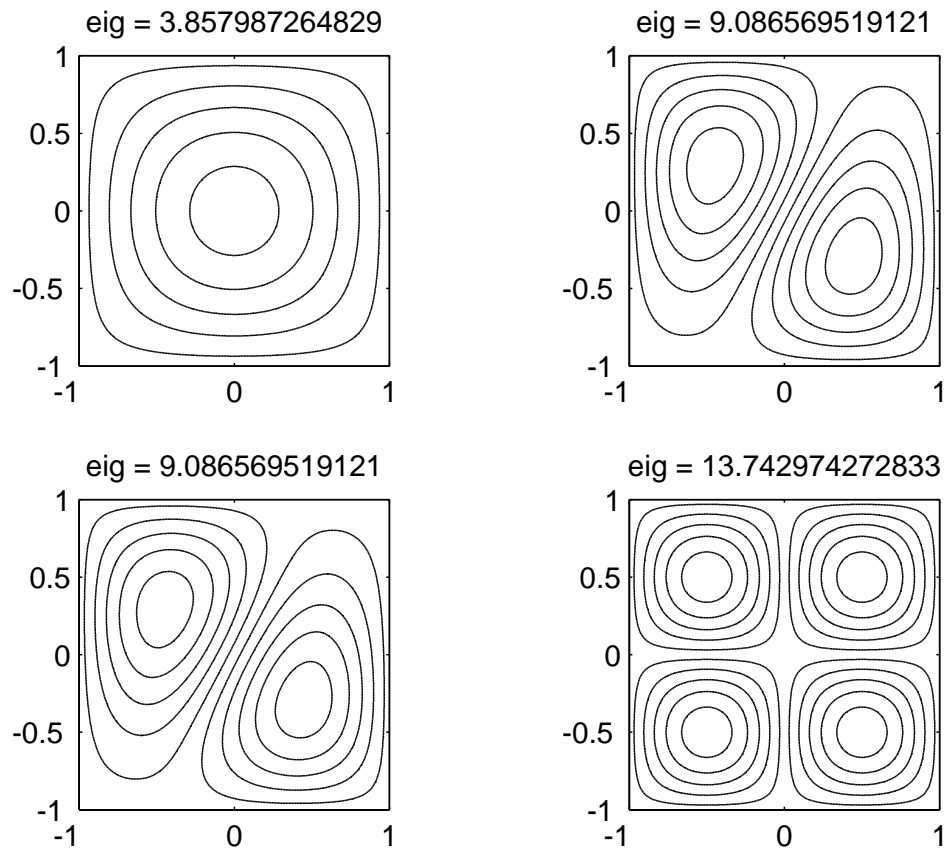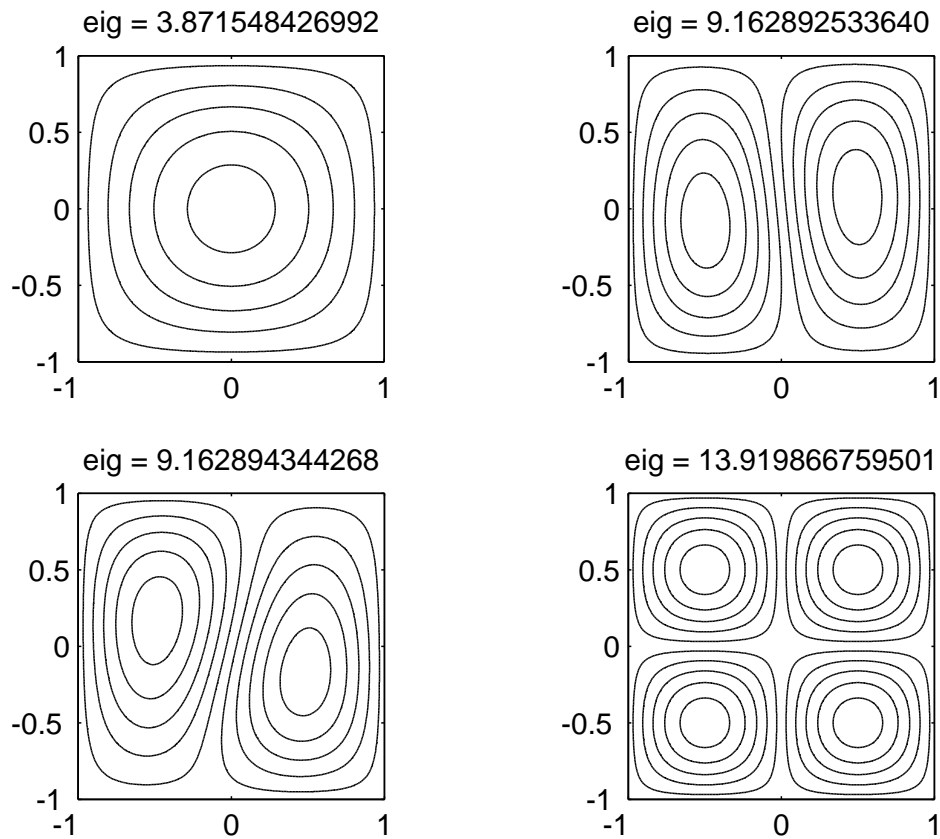
Fig. 15. First four buckling modes. Bi-axial buckling load of a simply supported 2-1-2 sandwich square plate with FG skins, $p = 0.5$, and using the sinusZZ0 theory.

Table 1

The present sinus theories.

theory	considers Zig-Zag effect	allows tichness-stretching
sinus	no	yes
sinus0	no	no
sinusZZ	yes	yes
sinusZZ0	yes	no

Table 2

Convergence study for the uni-axial buckling load of a simply supported 1-1-1 sandwich square plate with FG skins and $p = 1$ case using the sinus and sinusZZ theory.

grid	13^2	17^2	21^2
$\bar{P}$ sinus	6.31557	6.31502	6.31495
$\bar{P}$ sinusZZ	6.31474	6.31414	6.31406

Table 3

Uni-axial buckling $\bar{P}$ load of simply supported sandwich square plates with FG skins using the sinusoidal theory.

p	Theory	1-0-1	2-1-2	2-1-1	1-1-1	2-2-1	1-2-1
0	CLPT	13.73791	13.73791	13.73791	13.73791	13.73791	13.73791
	FSDPT	13.00449	13.00449	13.00449	13.00449	13.00449	13.00449
	TSDPT [10]	13.00495	13.00495	13.00495	13.00495	13.00495	13.00495
	SSDPT [29]	13.00606	13.00606	13.00606	13.00606	13.00606	13.00606
	sinus	12.95311	12.95311	12.95311	12.95311	12.95311	12.95311
	sinus0	13.00543	13.00543	13.00543	13.00543	13.00543	13.00543
	sinusZZ	12.95300	12.95196	12.95281	12.95203	12.95190	12.95310
	sinusZZ0	13.00532	13.00437	13.00515	13.00447	13.00427	13.00545
0.5	CLPT	7.65398	8.25597	8.56223	8.78063	9.18254	9.61525
	FSDPT	7.33732	7.91320	8.20015	8.41034	8.78673	9.19517
	TSDPT [10]	7.36437	7.94084	8.22470	8.43645	8.80997	9.21681
	SSDPT [29]	7.36568	7.94195	8.22538	8.43712	8.81037	9.21670
	sinus	7.16230	7.71642	7.98960	8.19279	8.55168	8.94166
	sinus0	7.18761	7.74350	8.01710	8.22139	8.58128	8.97284
	sinusZZ	7.16223	7.71597	7.98960	8.19183	8.55081	8.94150
	sinusZZ0	7.18755	7.74310	8.01710	8.22052	8.58039	8.97271
1	CLPT	5.33248	6.02733	6.40391	6.68150	7.19663	7.78406
	FSDPT	5.14236	5.81379	6.17020	6.43892	6.92571	7.48365
	TSDPT [10]	5.16713	5.84006	6.19394	6.46474	6.94944	7.50656
	SSDPT [29]	5.16846	5.84119	6.19461	6.46539	6.94980	7.50629
	sinus	5.06151	5.71145	6.05468	6.31499	6.78398	7.31966
	sinus0	5.07874	5.73041	6.07363	6.33558	6.80542	7.34331
	sinusZZ	5.06147	5.71123	6.05471	6.31414	6.78338	7.31949
	sinusZZ0	5.07869	5.73022	6.07366	6.33480	6.80476	7.34317
5	CLPT	2.73080	3.10704	3.48418	3.65732	4.21238	4.85717
	FSDPT	2.63842	3.02252	3.38538	3.55958	4.09285	4.71475
	TSDPT [10]	2.65821	3.04257	3.40351	3.57956	4.11209	4.73469
	SSDPT [29]	2.66006	3.04406	3.40449	3.58063	4.11288	4.73488
	sinus	2.63640	3.00755	3.36252	3.52992	4.05069	4.64692
	sinus0	2.64695	3.01855	3.37203	3.54149	4.06168	4.66043
	sinusZZ	2.63631	3.00698	3.35966	3.52994	4.05056	4.64688
	sinusZZ0	2.64687	3.01793	3.36937	3.54152	4.06160	4.66038
10	CLPT	2.56985	2.80340	3.16427	3.25924	3.79238	4.38221
	FSDPT	2.46904	2.72626	3.07428	3.17521	3.68890	4.26040
	TSDPT [10]	2.48727	2.74632	3.09190	3.19471	3.70752	4.27991
	SSDPT [29]	2.48928	2.74844	3.13443	3.19456	3.14574	4.38175
	sinus	2.47230	2.71991	3.06061	3.15730	3.66163	4.20546
	sinus0	2.48259	2.73058	3.06950	3.16827	3.67158	4.21787
	sinusZZ	2.47213	2.71679	3.05227	3.15658	3.66000	4.20449
	sinusZZ0	2.48242	2.72733	3.06150	3.16749	3.67015	4.21685

Table 4

Convergence study for the uni-axial buckling load of a simply supported 1-1-1 sandwich square plate with FG skins and $p = 1$ case using the sinus and sinusZZ theory.

grid	13^2	17^2	21^2
$\bar{P}$ sinus	1.68144	1.68127	1.68125
$\bar{P}$ sinusZZ	1.68002	1.67983	1.67981

Table 5

Bi-axial buckling load $\bar{P}$ of simply supported sandwich square plates with FG skins using the sinusoidal theory.

p	Theory	1-0-1	2-1-2	2-1-1	1-1-1	2-2-1	1-2-1
0	CLPT	6.86896	6.86896	6.86896	6.86896	6.86896	6.86896
	FSDPT	6.50224	6.50224	6.50224	6.50224	6.50224	6.50224
	TSDPT [10]	6.50248	6.50248	6.50248	6.50248	6.50248	6.50248
	SSDPT [29]	6.50303	6.50303	6.50303	6.50303	6.50303	6.50303
	sinus	6.47656	6.47656	6.47656	6.47656	6.47656	6.47656
	sinus0	6.50272	6.50272	6.50272	6.50272	6.50272	6.50272
	sinusZZ	6.47650	6.47598	6.47641	6.47601	6.47595	6.47655
	sinusZZ0	6.50266	6.50219	6.50258	6.50224	6.50214	6.50272
0.5	CLPT	3.82699	4.12798	4.28112	4.39032	4.59127	4.80762
	FSDPT	3.66866	3.95660	4.10007	4.20517	4.39336	4.59758
	TSDPT [10]	3.68219	3.97042	4.11235	4.21823	4.40499	4.60841
	SSDPT [29]	3.68284	3.97097	4.11269	4.21856	4.40519	4.60835
	sinus	3.58115	3.85821	3.99480	4.09640	4.27584	4.47083
	sinus0	3.59380	3.87175	4.00855	4.11069	4.29064	4.48642
	sinusZZ	3.58112	3.85799	3.99480	4.09592	4.27541	4.47075
	sinusZZ0	3.59377	3.87155	4.00855	4.11026	4.29020	4.48636
1	CLPT	2.66624	3.01366	3.20195	3.34075	3.59831	3.89203
	FSDPT	2.57118	2.90690	3.08510	3.21946	3.46286	3.74182
	TSDPT [10]	2.58357	2.92003	3.09697	3.23237	3.47472	3.75328
	SSDPT [29]	2.58423	2.92060	3.09731	3.23270	3.47490	3.75314
	sinus	2.53076	2.85573	3.02734	3.15750	3.39199	3.65983
	sinus0	2.53937	2.86520	3.03681	3.16779	3.40271	3.67165
	sinusZZ	2.53073	2.85562	3.02735	3.15707	3.39169	3.65975
	sinusZZ0	2.53935	2.86511	3.03683	3.16740	3.40238	3.67158
5	CLPT	1.36540	1.55352	1.74209	1.82866	2.10619	2.42859
	FSDPT	1.31921	1.51126	1.69269	1.77979	2.04642	2.35737
	TSDPT [10]	1.32910	1.52129	1.70176	1.78978	2.05605	2.36734
	SSDPT [29]	1.33003	1.52203	1.70224	1.79032	2.05644	2.36744
	sinus	1.31820	1.50377	1.68126	1.76496	2.02535	2.32346
	sinus0	1.32348	1.50927	1.68601	1.77075	2.03084	2.33022
	sinusZZ	1.31816	1.50349	1.67983	1.76497	2.02528	2.32344
	sinusZZ0	1.32344	1.50897	1.68469	1.77076	2.03080	2.33019
10	CLPT	1.28493	1.40170	1.58214	1.62962	1.89619	2.19111
	FSDPT	1.23452	1.36313	1.53714	1.58760	1.84445	2.13020
	TSDPT [10]	1.24363	1.37316	1.54595	1.59736	1.85376	2.13995
	SSDPT [29]	1.24475	1.37422	1.56721	1.59728	1.57287	2.19087
	sinus	1.23615	1.35996	1.53030	1.57865	1.83081	2.10273
	sinus0	1.24130	1.36529	1.53475	1.58414	1.83579	2.10893
	sinusZZ	1.23606	1.35840	1.52613	1.57829	1.83000	2.10224
	sinusZZ0	1.24121	1.36367	1.53075	1.58374	1.83508	2.10843